Biophysical Journal, Volume *115*

Supplemental Information

Cooperative Induction of Ordered Peptide and Fatty Acid Aggregates

Radoslaw Bomba, Witek Kwiatkowski, Antoni Sánchez-Ferrer, Roland Riek, and Jason Greenwald

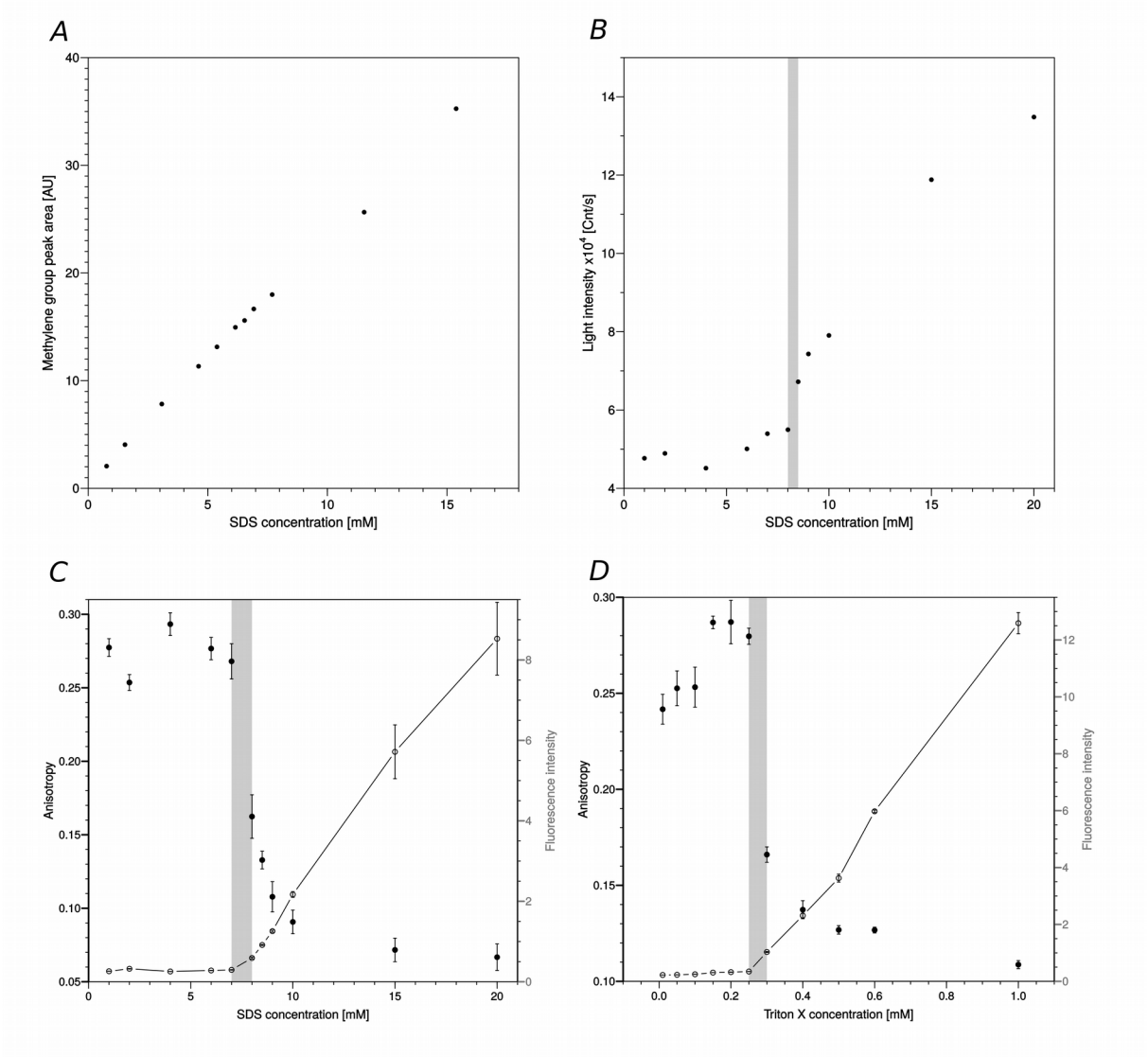

Figure S1. Controls for three analytical methods used in the determination of amphiphile critical aggregation concentrations. Panel *A* represents NMR measurements utilizing peak areas of the methylene groups of SDS in ^{1}H NMR spectra. The signal is proportional to the concentration of SDS in the whole range above and below its CMC (literature value: 8.2 mM), confirming that this technique is only appropriate for the determination of the CVC of vesicle forming amphiphiles and not their CMC. Panel *B* represents the intensity of scattered light as a function of SDS concentration. For the concentrations below the CMC, the signal is low and constant. Above the CMC, the signal increases significantly. The CMC was determined to lie within the range of concentrations at which there was a change of the trend of the data: 8–8.5 mM. Panels *C* and *D* represents data used to determine the CMCs of SDS and Triton X-100 by DPH fluorescence polarization anisotropy and fluorescence intensity. The initially high anisotropy for DPH alone is due to large aggregates that decrease in size near the CMC through a partial solubilization by micelles with a concomitant increase in fluorescence intensity. The CMC values for SDS and Triton X-100 determined with this method are 7–8 mM and 0.25–0.3 mM, respectively.

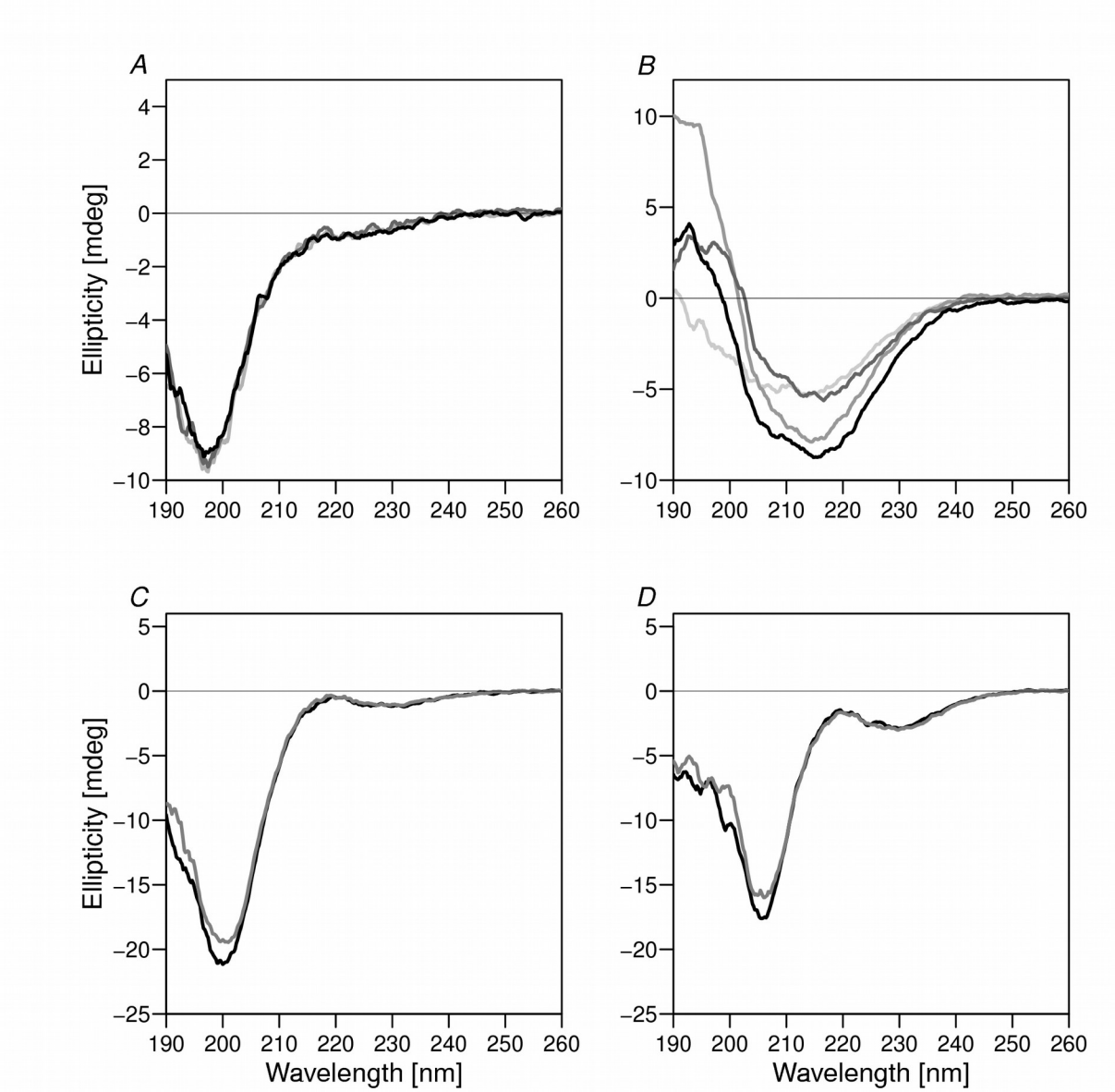

Figure S2. Concentration, time and pH dependence of $(OV)_4$ secondary structure. Panel *A* depicts the CD spectra of $(OV)_4$ at our standard conditions (0.5 mg/ml, pH 7.8) measured immediately after preparation (light grey line), 1 hour after preparation (dark grey line) and after 24 hours (black line). Panel *B* represents the spectra of $(OV)_4$ at pH 11 measured immediately (light grey line), after 1 hour (grey line), after 30 hours (dark grey line) and after 54 hours (black line). Differences in the spectra in *B* can be due to uneven or changing distribution of the aggregates sizes in the sample. Panels *C* and *D* depict the spectra of $(OV)_4$ at 2 mg/ml and 5 mg/ml, respectively. The black lines correspond to the entire solution and grey lines to the supernatant after centrifugation at 130k g. No change in the spectra before and after centrifugation indicates that at these concentrations the peptide is soluble. Nevertheless, at 5 mg/ml the CD spectrum is different from that at 2 mg/ml and also no longer typical for random coil or any other secondary structure.

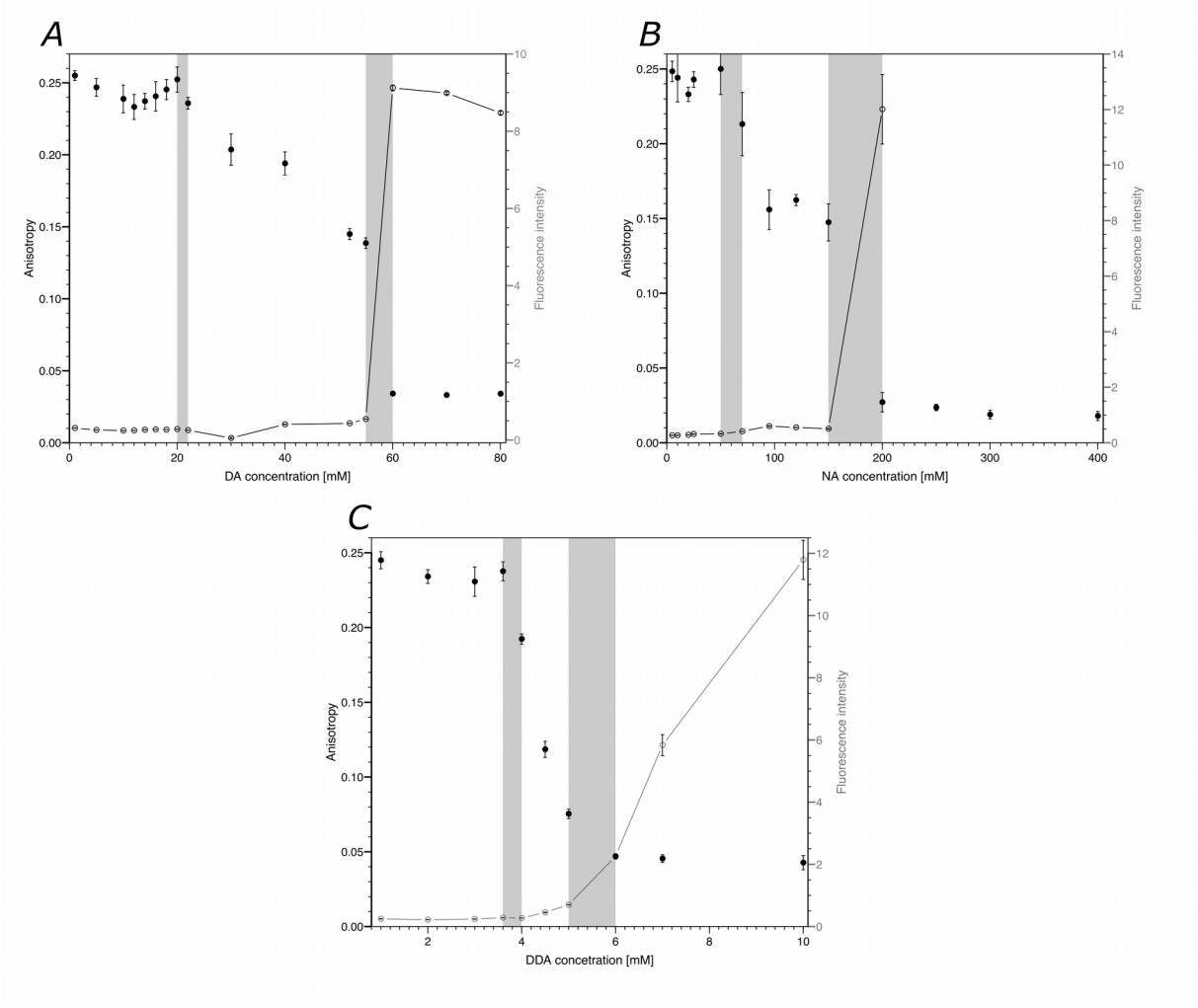

Figure S3. Determination of fatty acid CMC and CVC via DPH fluorescence. The fluorescence polarization anisotropy (black circles) and fluorescence intensity (empty circles) of DPH in NA (*A*), DA (*B*) and DDA (*C*) solutions at different concentrations at pH 7.8 are plotted. Each fatty acid shows two transitions, marked as the grey bands in the plots, that are delineated by the decrease of anisotropy and increase of fluorescence intensity. The first transition corresponds to the CMC and the second one to the CVC. The error bars represent the standard deviation from 10 measurements.

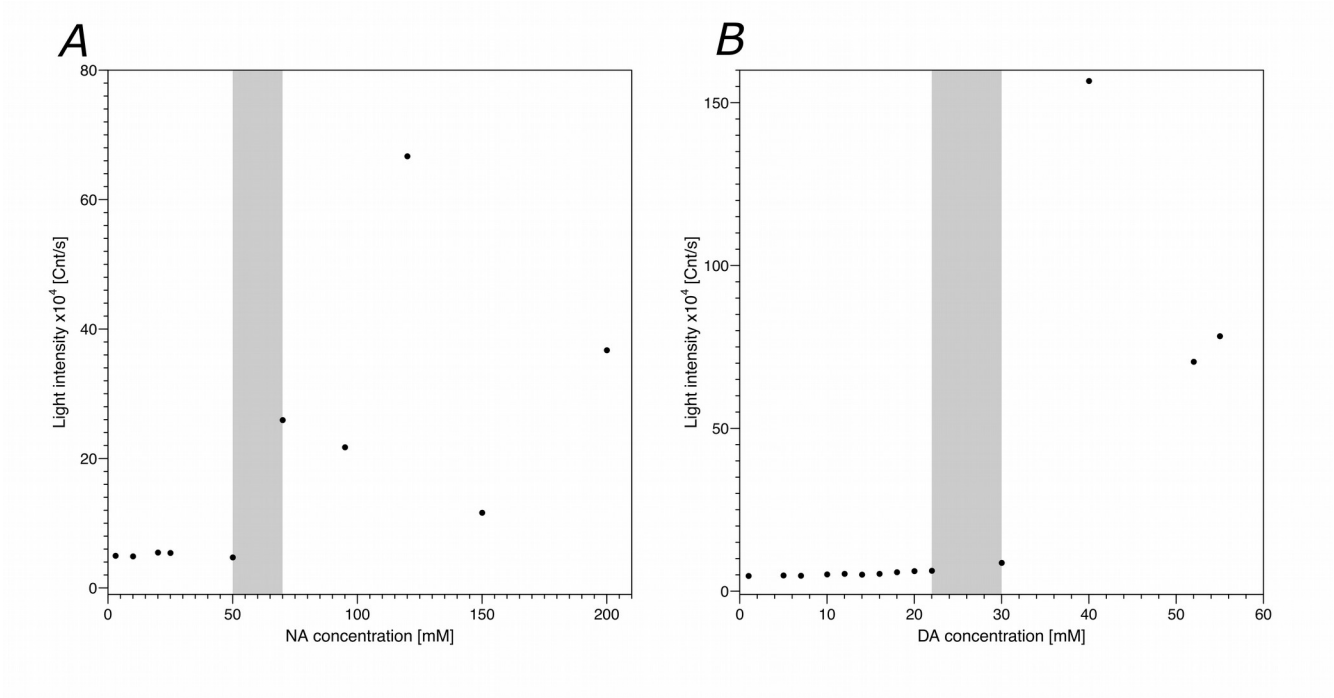

Figure S4. Determination of fatty acid CMC using scattered light intensity. Panel *A* represents measurements for NA and panel *B* for DA. The transition of fatty acids from monomers to micelles leads to an increase in the intensity of scattered light as well as to large fluctuations of the signal. The grey bar indicates the region of uncertainty in the CMC for these measurements.

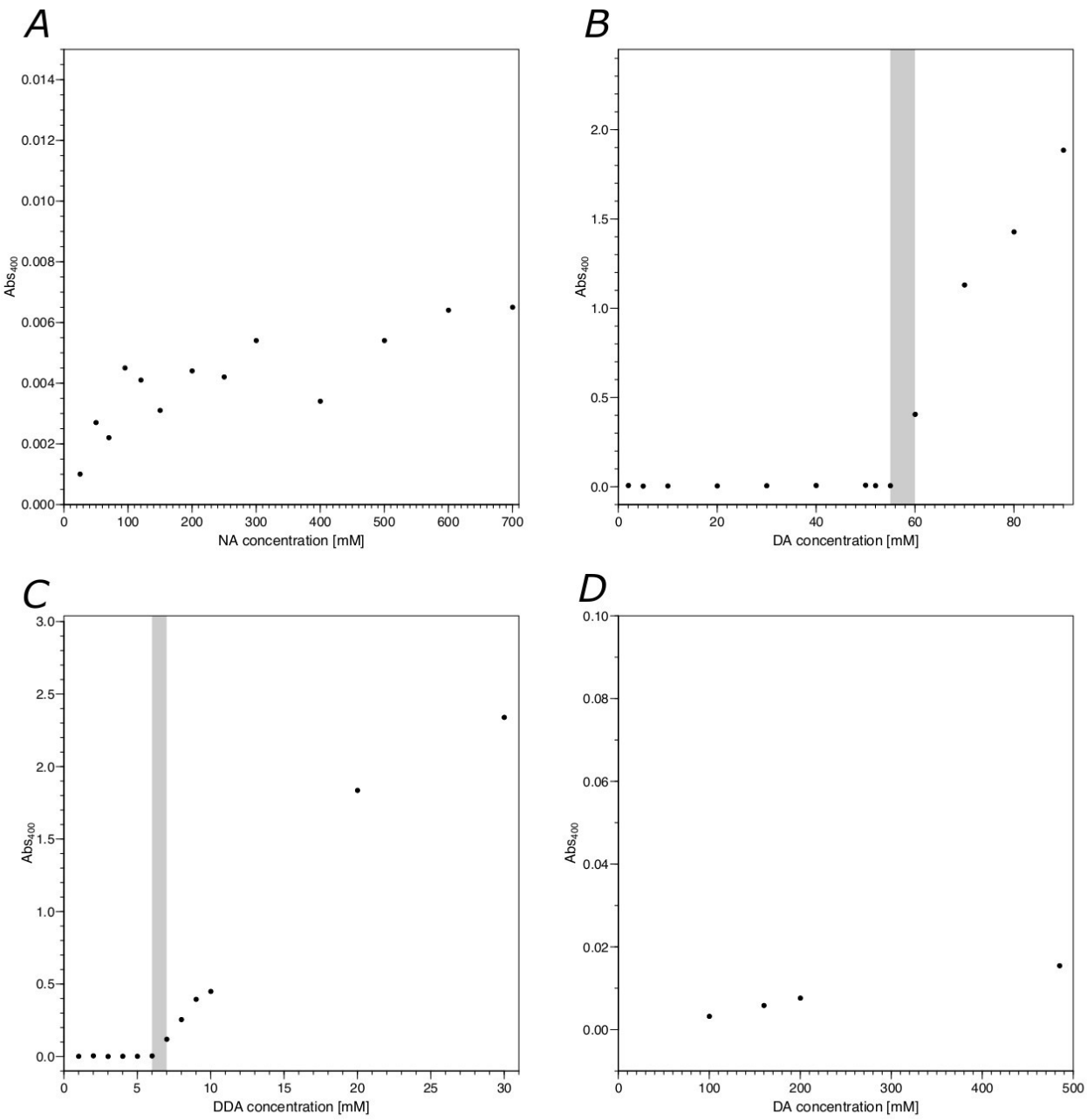

Figure S5. Determination of fatty acid CVC using turbidity of vesicular solutions. The figures plot the absorbance at 400 nm of NA (*A*), DA (*B*) and DDA (*C*) solutions at different fatty acid concentrations at pH 7.8. The increase of absorbance indicates the transition from micellar to the vesicular state of fatty acids (marked with grey bands). Figure *D* represents DA solutions at pH 8.2. In the case of NA at pH 7.8 and DA at pH 8.2 no transition to vesicles could be detected.

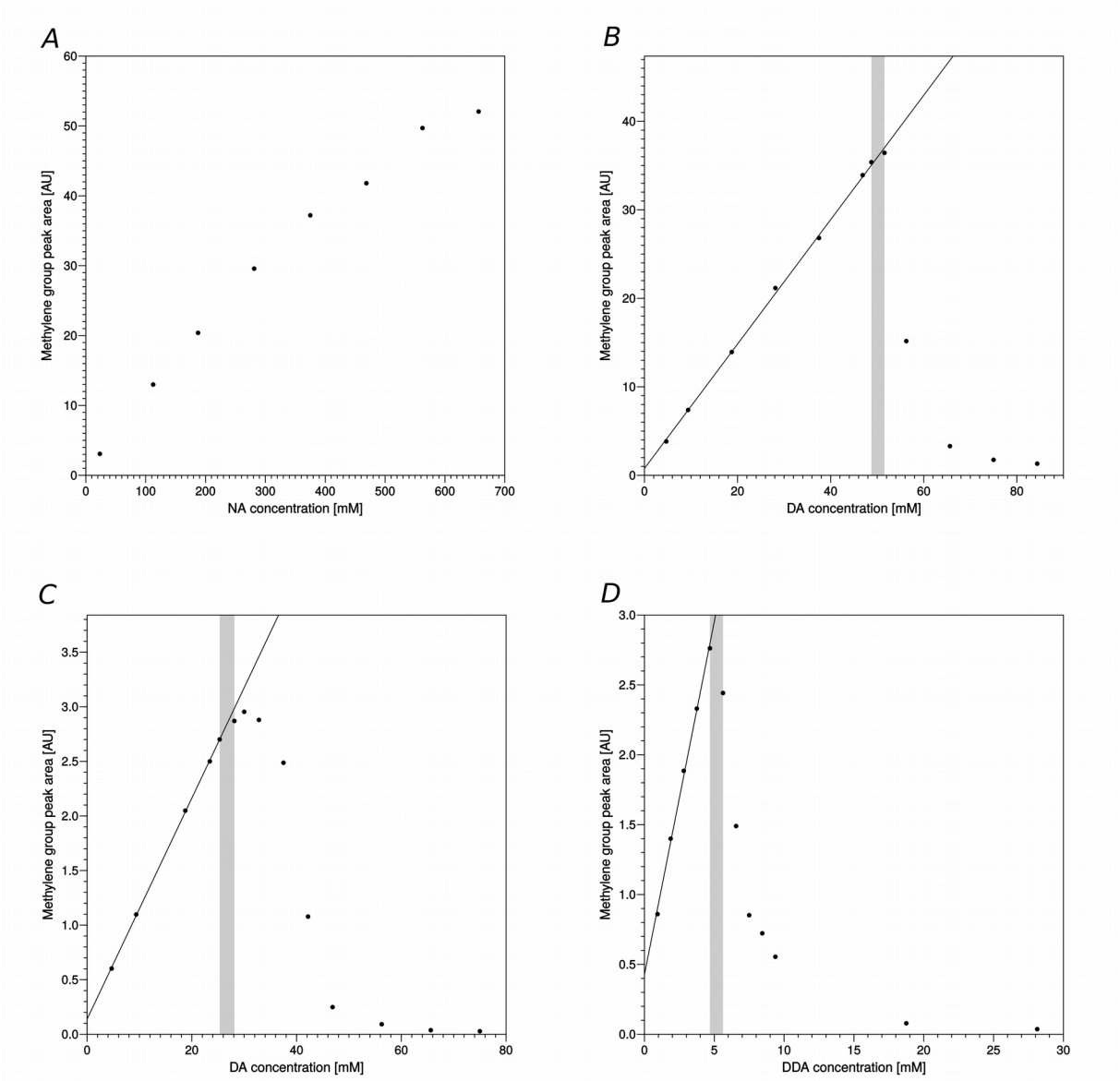

Figure S6. Determination of fatty acid CVC using NMR signal intensity. The CVC of NA (*A*), DA (*B*), and DDA (*D*) at pH 7.8 and DA at pH 7.4 (*C*) determined by 1D ^{1}H NMR spectroscopy. The CVCs were determined as the concentration at which the methylene peak area started to deflect from the linear relation with concentration. The decrease of peak area is attributed to the fast exchange of fatty acid molecules with vesicles. The uncertainty in ranges of CVC values based on this data are marked with grey bands. In the case of NA, the peak area started to deflect from a linear increase above 300 mM NA, however no clear transition was detectable with this technique. In *B* compared to *C* we confirmed that in the more acidic conditions, the CVC of DA is significantly lower (25-28 mM) than at higher pH (49-52 mM).

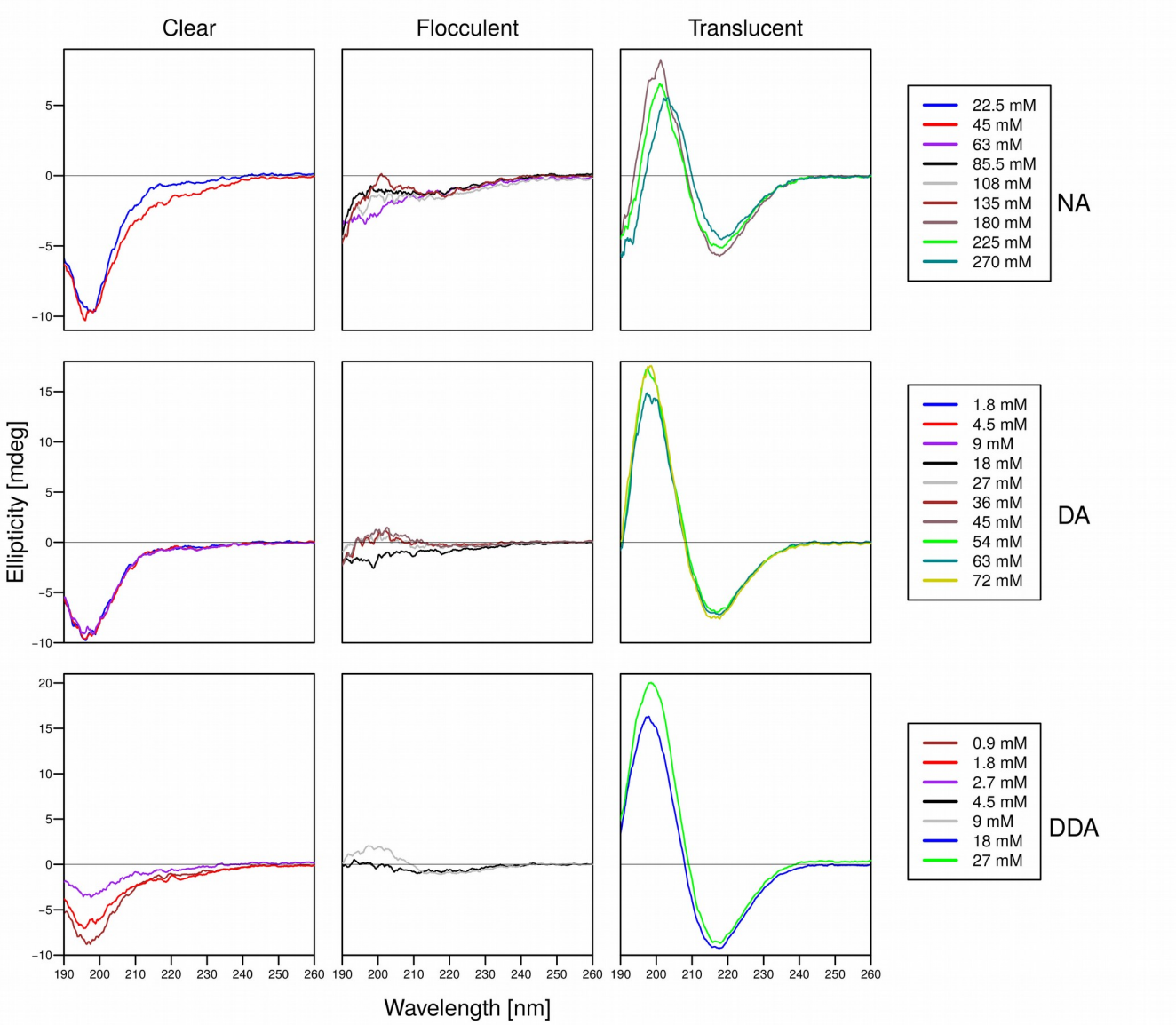

Figure S7. CD spectra of $(OV)_4$ in various fatty acid solutions. The top three plots are the spectra of $(OV)_4$ in various concentrations of NA, the middle three in DA and the bottom three in DDA. The left plots are spectra of optically clear mixtures at lower concentration of fatty acid indicating that the peptide adopts a random coil structure. The middle plots are the spectra from samples that show a flocculent precipitate and little to no CD signal. The right plots are the spectra from samples that are translucent and exhibit a β-structure CD signature. The legends to the right of the plots indicate the concentrations of fatty acids, highlighting that for all three fatty acid-peptide mixtures, the peptide has three different fatty acid concentration-dependent states.

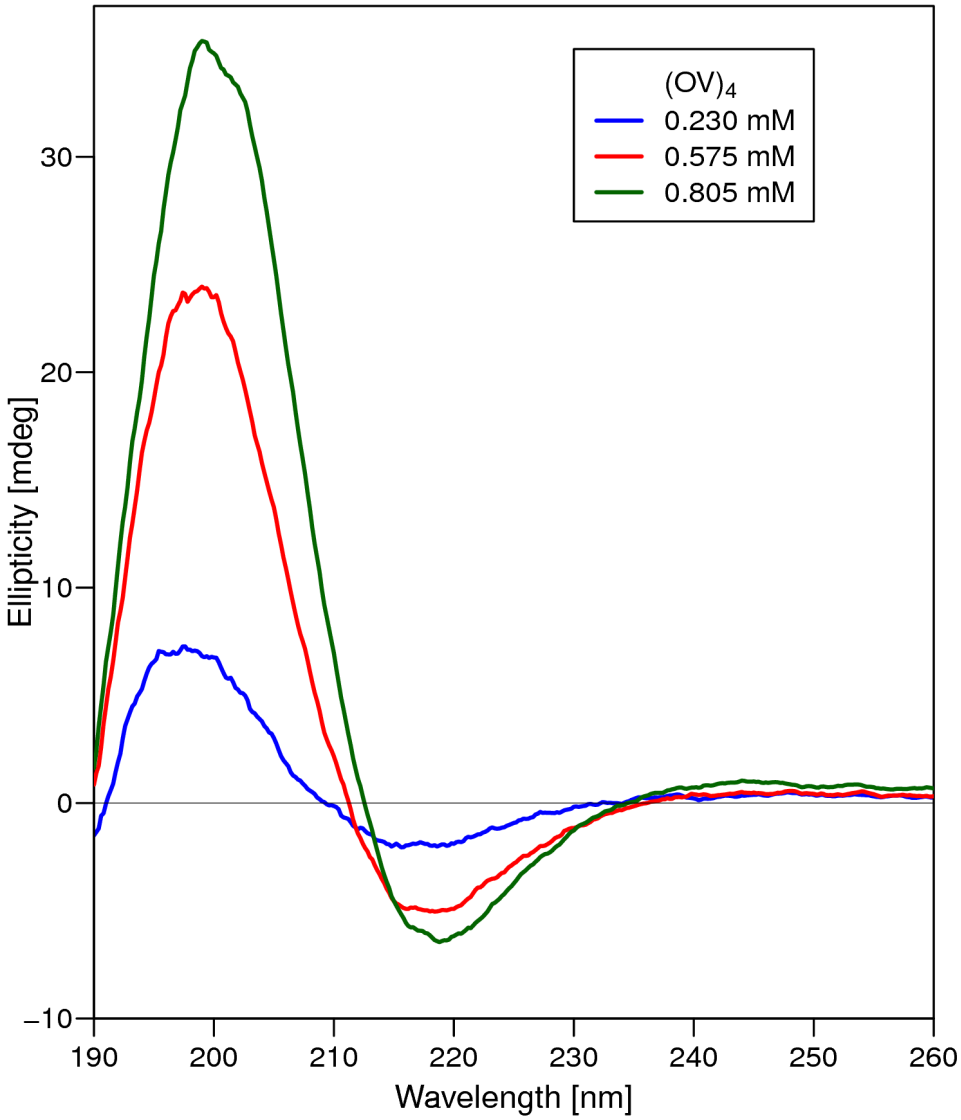

Figure S8. CD spectra of $(OV)_4$-DA translucent precipitates at different concentrations of $(OV)_4$. Three samples were prepared at three concentrations of $(OV)_4$ with 72 mM DA at pH 7.8. All of the spectra indicate that $(OV)_4$ adopts β-strand structure and the visual appearance of the translucent mixture is the same for all three samples.

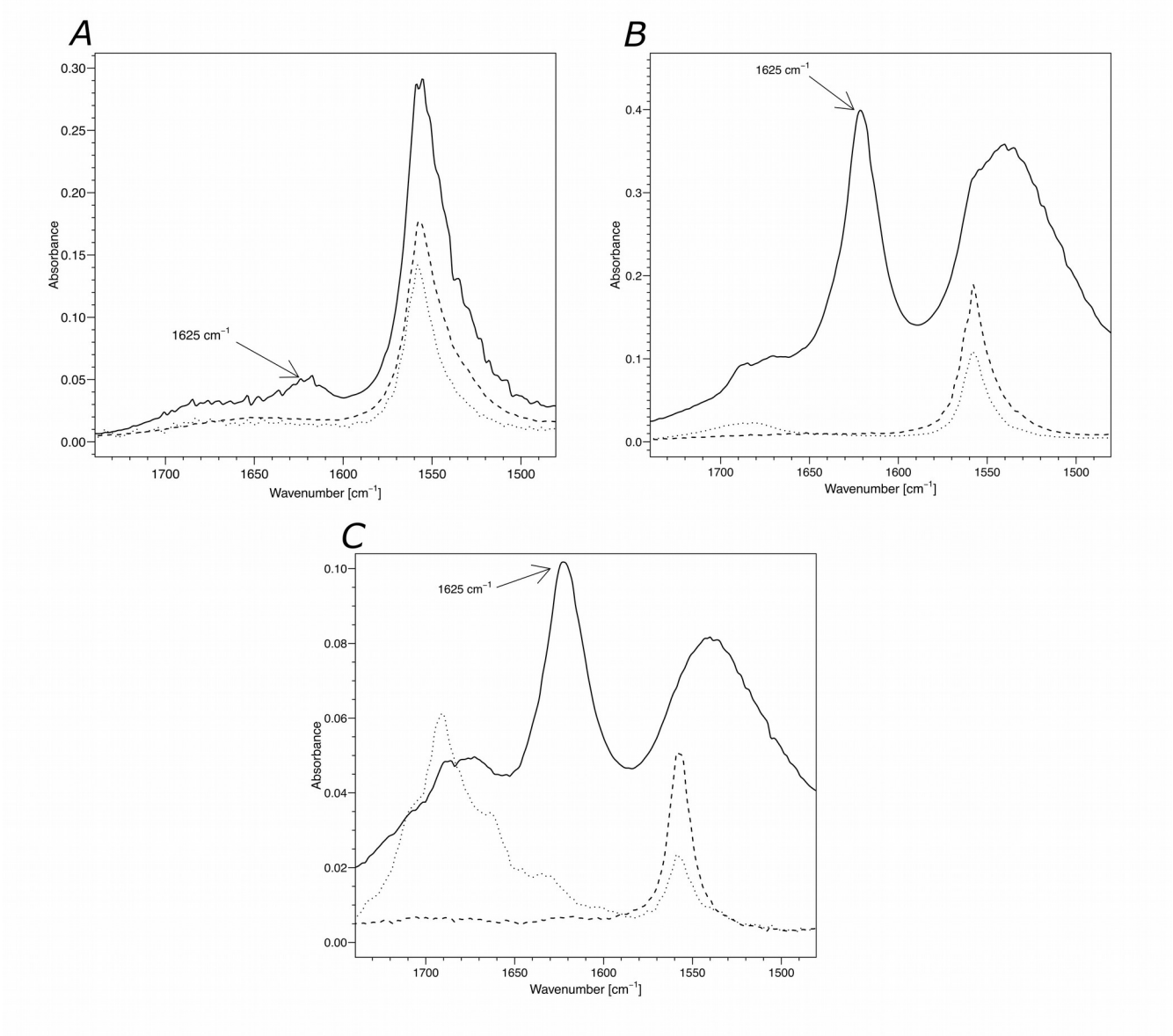

Figure S9. FTIR spectra of $(OV)_4$-fatty acid flocculent precipitates. Samples of the flocculent precipitates with NA (*A*), DA (*B*) and DDA (*C*) were centrifuged at 25k g for 5 min and the precipitate resuspended in 4 µl of the supernatant which was applied to the ATR cell and air-dried. The arrows indicate the absorbance bands at 1625 cm^{-1} characteristic for the β-strand structure of the peptides. Black traces correspond to flocculent precipitate, dotted lines are the spectra measured for the dried supernatant and dashed lines show spectra of dried fatty acid solutions without peptide.

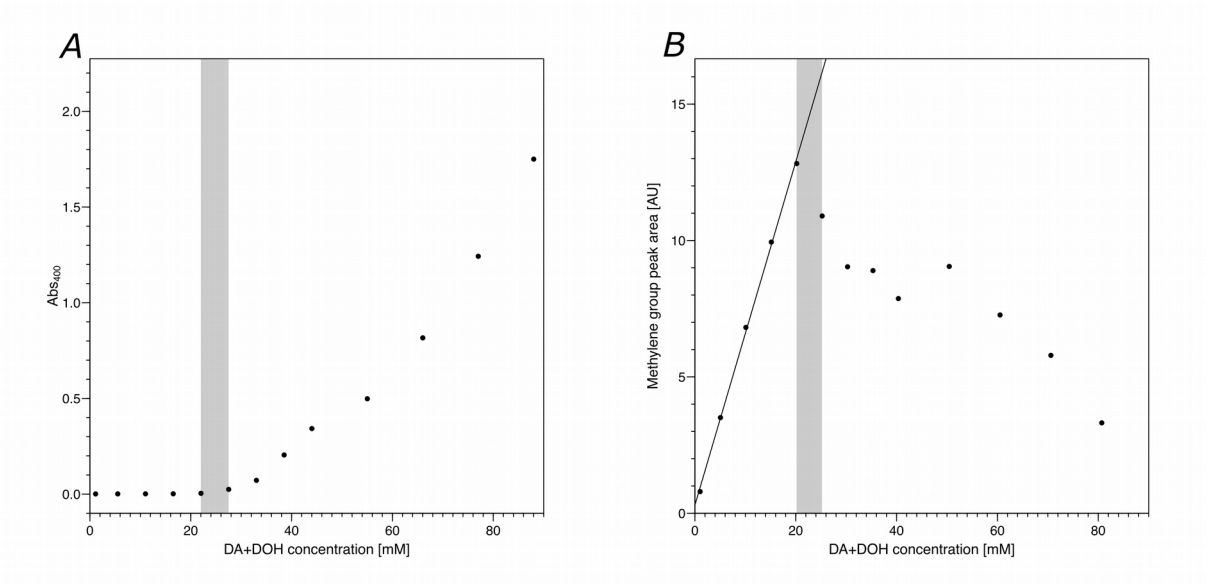

Figure S10. CVC measurements of DA:DOH solutions. The CVC of the 10:1 DA:DOH solution was determined by turbidity measurements (*A*) as in Fig. S5 and 1D ^{1}H NMR measurements (*B*) as in Fig. S6. The two techniques are in good agreement with a CVC of 20-22 mM total amphiphile.

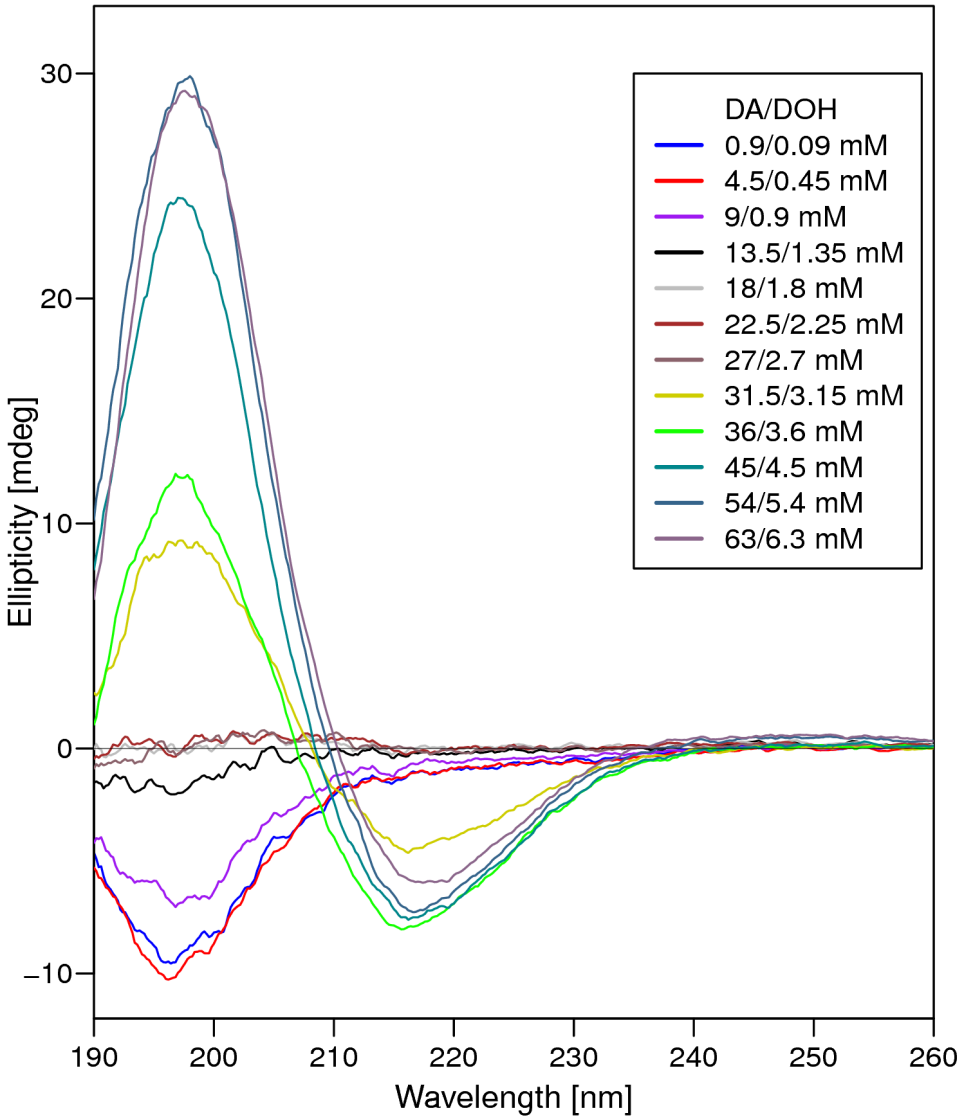

Figure S11. Decanoic acid:decanol solution has a lower transition concentration for the translucent precipitate. The CD spectra of $(OV)_4$ mixtures with a range of concentrations of decanoic acid:decanol (10:1) show that the transition from flocculent precipitate to translucent precipitate occurs near 35 mM of amphiphiles. This value is significantly lower than for decanoic acid alone (54 mM) and parallels the change in the CVC of decanoic acid in the presence of decanol.

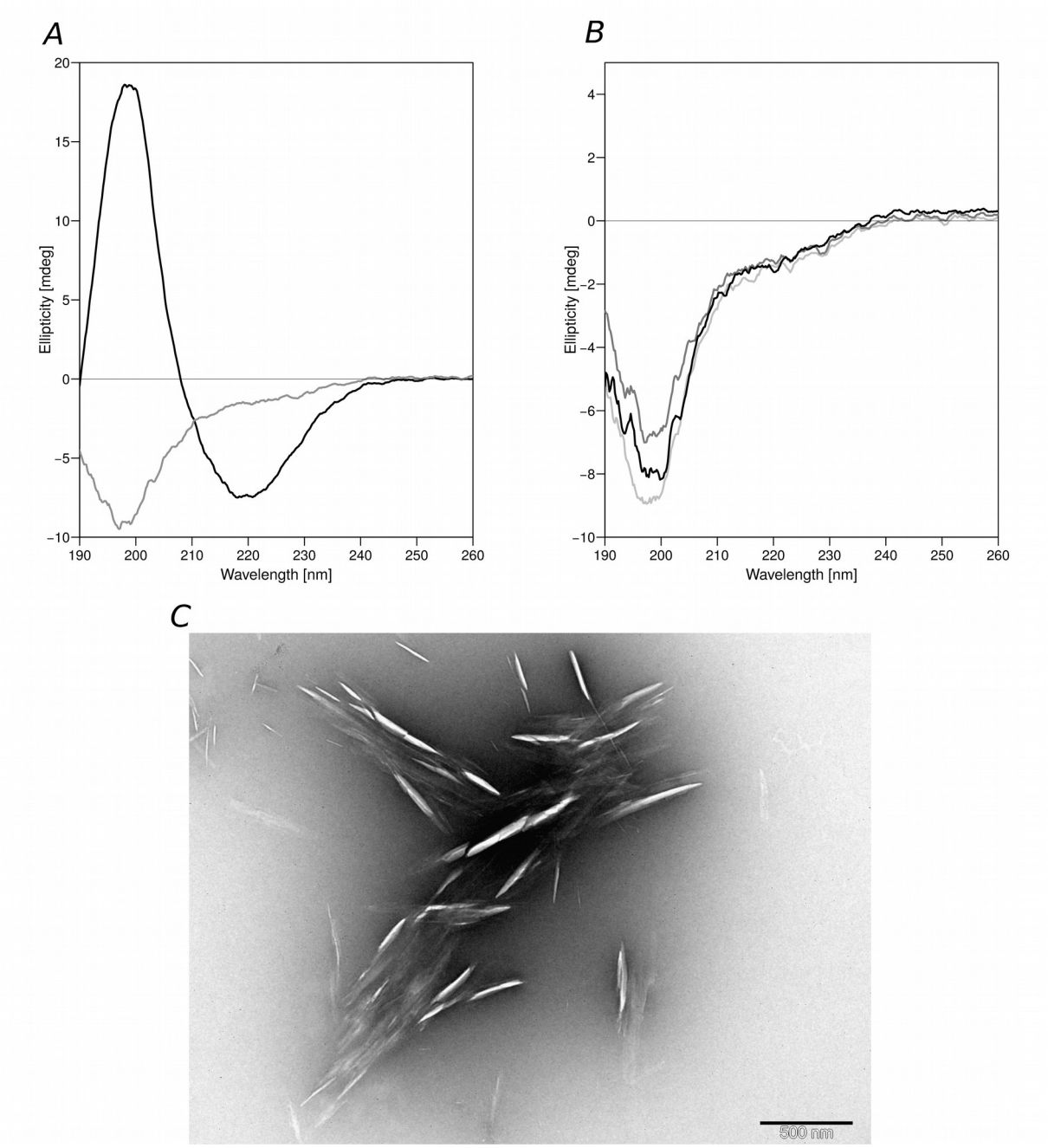

Figure S12. Characterization of Ac-V(DV)$_4$-NH$_2$ in decanoic acid solutions. Panel *A* depicts the CD of 575 μM Ac-V(DV)$_4$-NH$_2$ at pH 7.8 (grey line) and pH 3.5 (black line) indicating that at neutral pH, the peptide adopts random coil conformation, while in acidic conditions it adopts a β-structure. Panel *B* represents three CD spectra of 575 μM Ac-V(DV)$_4$-NH$_2$ in the presence of decanoic acid at 9 mM (light grey line), 18 mM (dark grey line) and 72 mM (black line), indicating that the peptide structure is neither sensitive to the presence of fatty acid nor the fatty acid aggregation state. Image *C* shows the electron micrograph of the amyloids formed by Ac-V(DV)$_4$-NH$_2$ at pH 3.5.

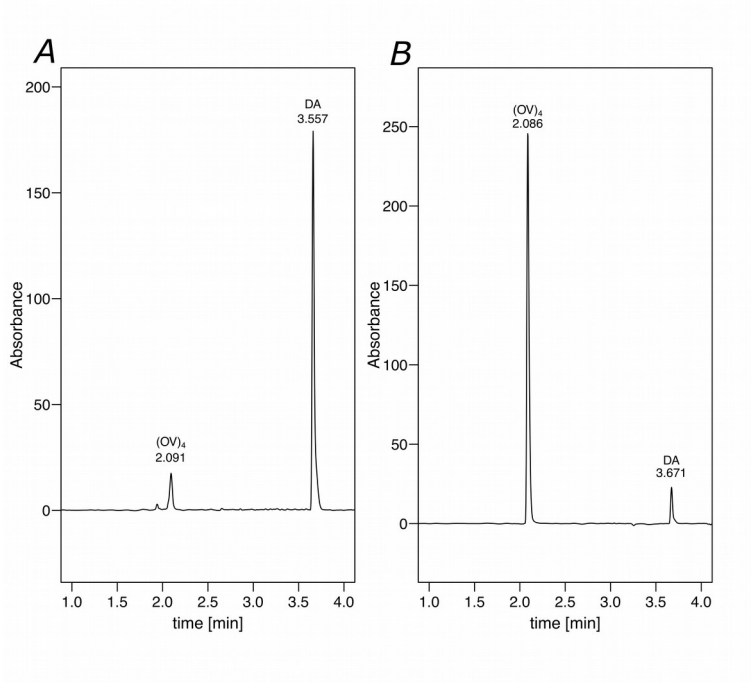

	90 mM NA + 575µM $(OV)_4$ (100.4 µl)			225 mM NA + 1000µM $(OV)_4$ (96 µl)		
	Flocculent precipitate	Supernatant	Total	Translucent precipitate	Supernatant	Total
$(OV)_4$ quantity [mmol]	$5.29x10^{-2}$	$4.26x10^{-3}$	$5.72x10^{-2}$	$8.41x10^{-2}$	$1.71x10^{-2}$	$9.93x10^{-2}$
Fatty acid quantity [mmol]	0.141	8.21	8.35	0.621	22.0	22.6
Fatty acid / $(OV)_4$	**2.66**			**7.38**		
	27 mM DA + 575µM $(OV)_4$ (100 µl)			63 mM DA + 750µM $(OV)_4$ (89.3 µl)		
	Flocculent precipitate	Supernatant	Total	Translucent precipitate	Supernatant	Total
$(OV)_4$ quantity [mmol]	$5.49x10^{-2}$	$2.31x10^{-3}$	$5.72x10^{-2}$	$6.19x10^{-2}$	$1.15x10^{-2}$	$7.34x10^{-2}$
Fatty acid quantity [mmol]	0.174	2.41	2.58	0.442	4.99	5.43
Fatty acid/ $(OV)_4$	**3.17**			**7.14**		

Figure S13. Determination of the molar ratio of fatty acids to $(OV)_4$ in flocculent and translucent precipitates. Chromatograms for the reverse phase analysis of the supernatant (*A*) and flocculent precipitate (*B*) of DA-$(OV)_4$ mixture showing good separation of both species. The table summarizes the HPLC quantified amount of fatty acids and peptide in the various precipitates and their supernatants. The volumes of the analyzed mixtures and concentrations of fatty acids are also given.

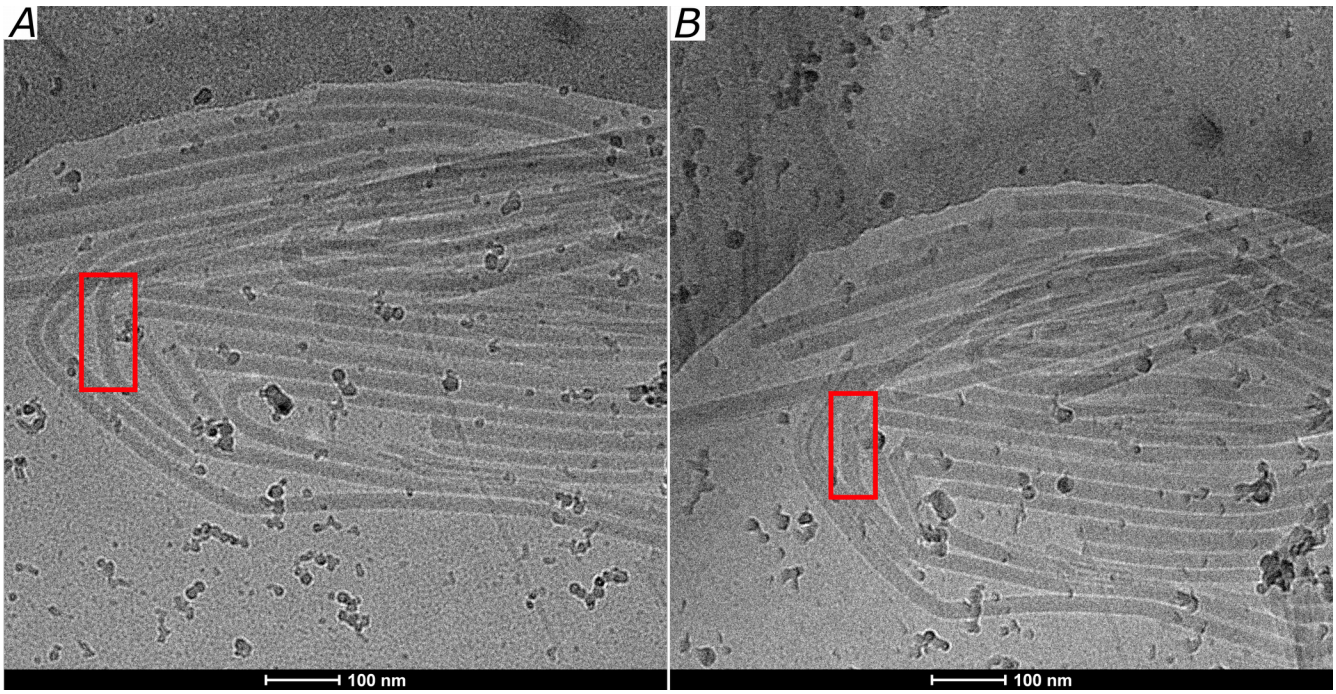

Figure S14. Tilted Cryo-TEM images of DA-$(OV)_4$ tube-like aggregates. The sample was tilted by 0 degrees (*A*) and by 40 degrees (*B*). The red box shows a feature that is parallel to the rotation axis. Thickness of this feature was measured resulting in 22.6 nm for not tilted sample, and 23.0 nm after tilting by 40 degrees. The same width before and after tilting indicates that those structures are not flat ribbons but rather rod- or tube-like.

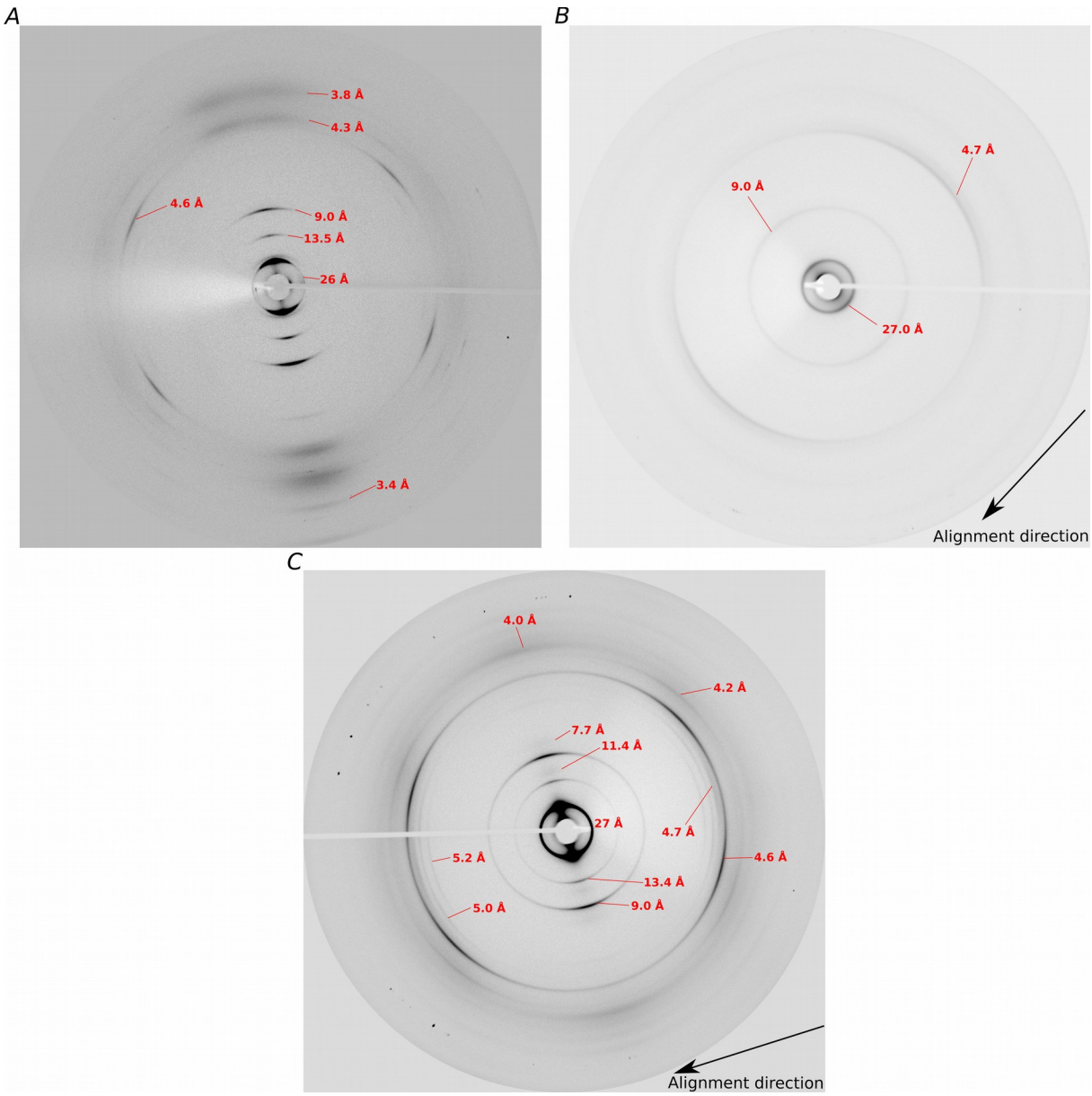

Figure S15. X-ray diffraction patterns of aligned decanoic acid and $(OV)_4$ samples. Panel *A* is a DA solution that has been dried into a flat disc inside of a nylon loop. Panel *B* is the image from aligned fibrils of $(OV)_4$ formed at pH 11. Panel *C* is the image from the aligned DA-$(OV)_4$ assemblies from a translucent precipitate. The dominant features in *A* and *C* arise from the DA bilayer while the weak equatorial reflections at 11.4 Å and 7.7 Å and meridional reflection at 4.7 Å are uniquely present in the translucent precipitate. Based on these features we can conclude that $(OV)_4$ adopts a cross-β-sheet in both pH 11 fibrils and the assemblies with decanoic acid.

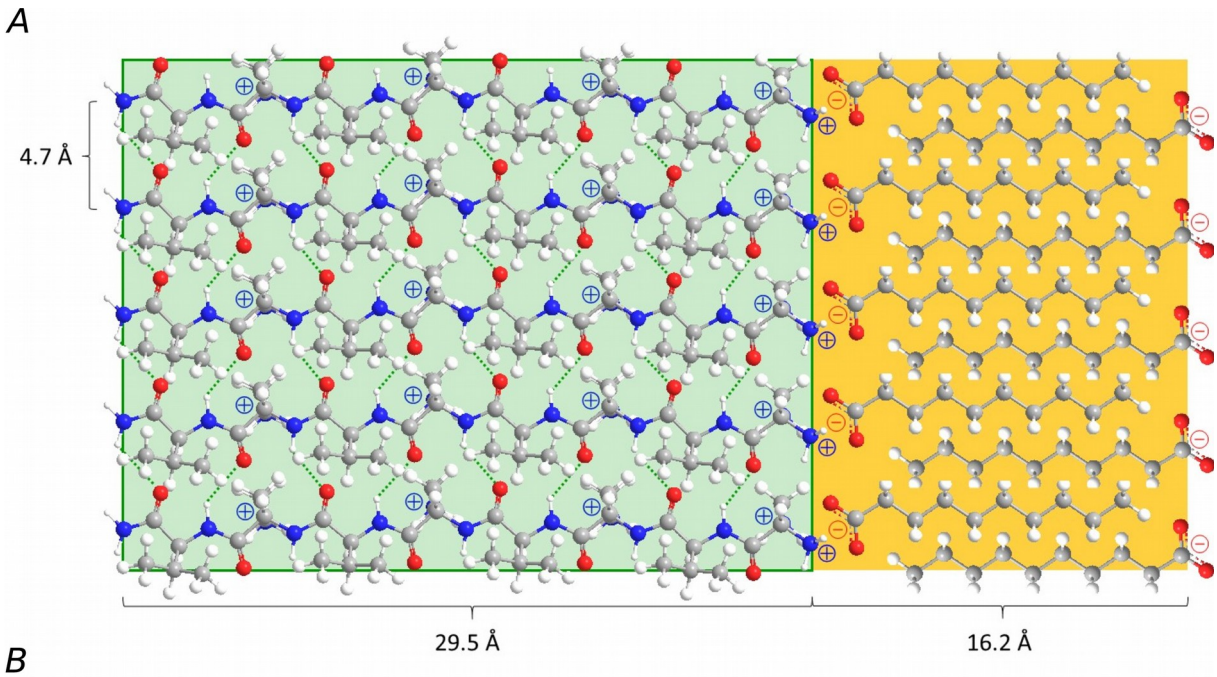
A
4.7 Å
29.5 Å
16.2 Å

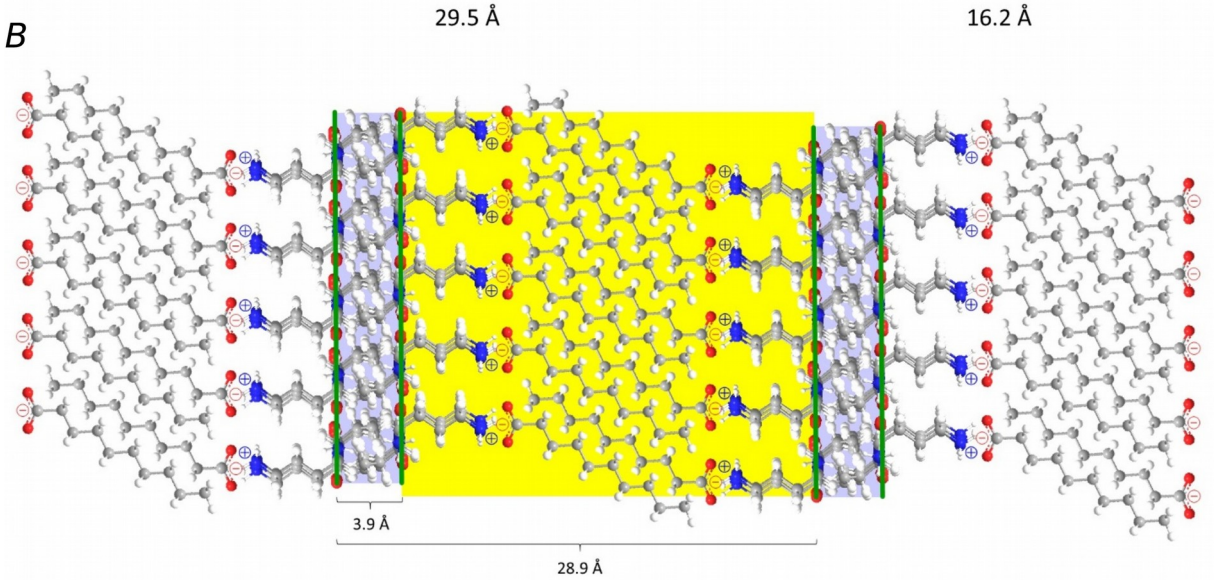
B
3.9 Å
28.9 Å

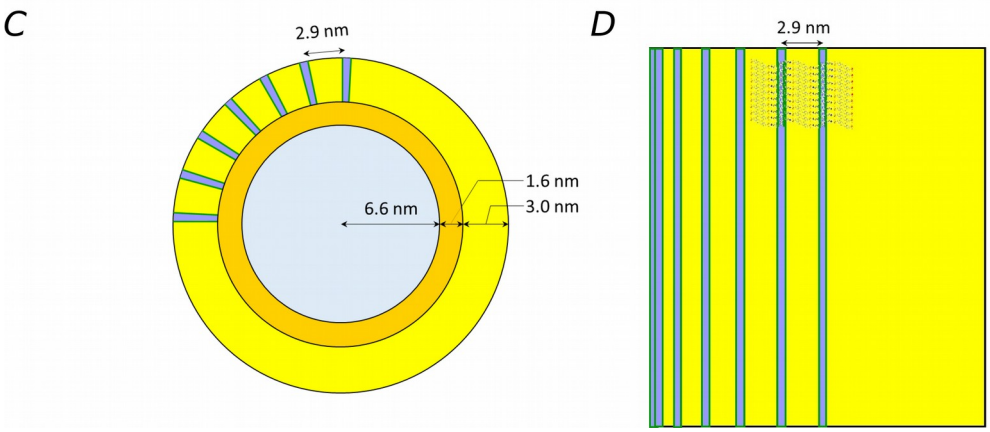
C
2.9 nm
6.6 nm
1.6 nm
3.0 nm
D
2.9 nm

Figure S16. Mode of self-assembly of the DA-$(OV)_4$ tubes. (*A*) Side view of a model showing a single parallel β-sheet of the peptide domain (green), and the deprotonated and interdigitated DA bilayer domain (orange). The valine side chains point out of the page and the ornithine residues point into the page (not visible in this view). The two domains are connected by ionic interactions. (*B*) View 90 degrees from *A* showing the radially distributed mode of self-assembly of the DA-$(OV)_4$ tubes. Two β-sheets (green lines) are held together by Van der Waals interactions between valine side chains (blue), and the pairs of sheets are connected through ionic interactions between the protonated ornithine residues and a deprotonated and interdigitated DA bilayer (in yellow). (*C*) cross-section and (*D*) lateral perspective of the hollow core-two-shell cylinder structure (the colors represent the different domains as depicted in panel *A* and *B)*.

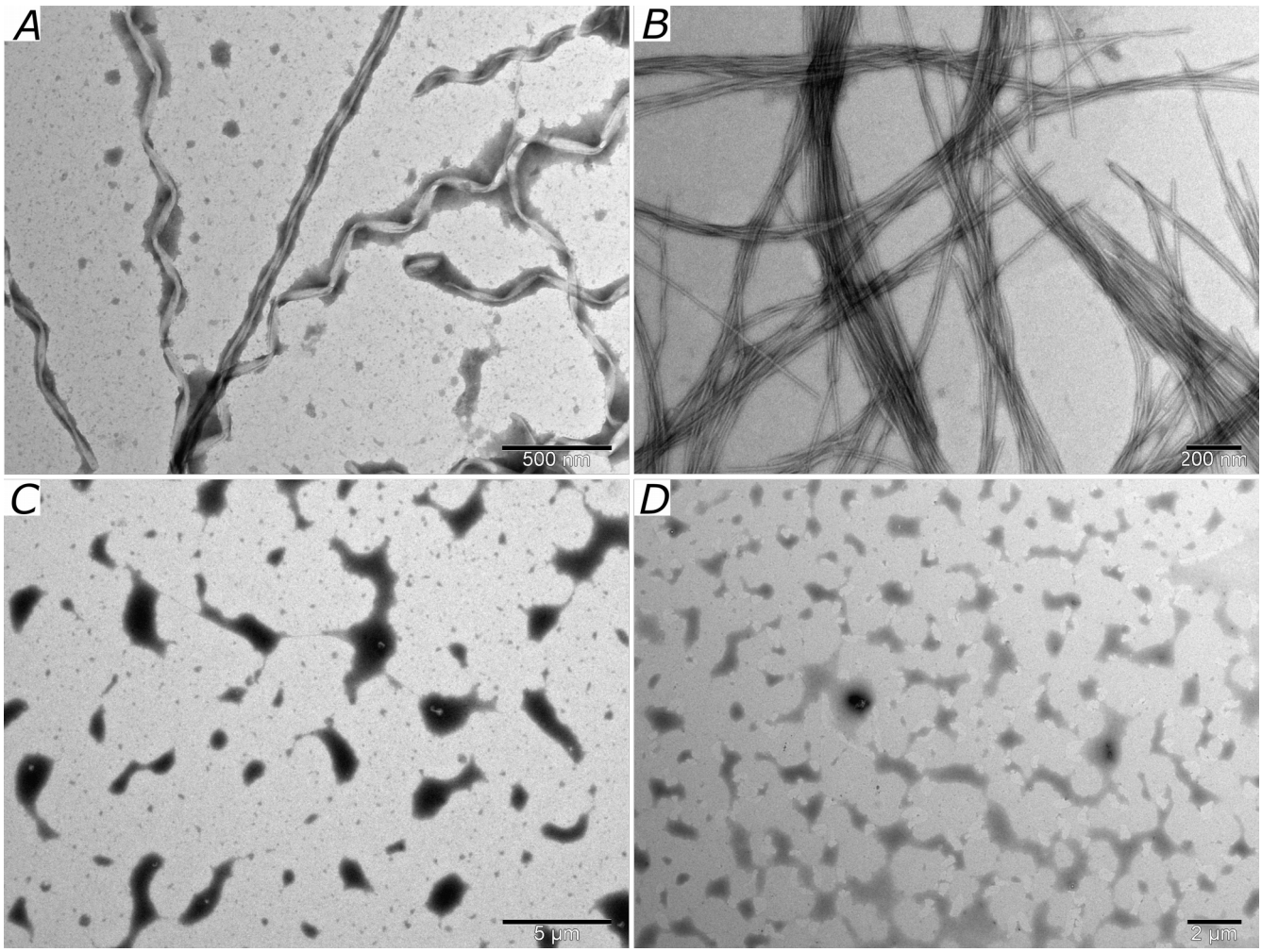

Figure S17. Subtle amino acid sequence differences of a peptide yield a mesoscopic structural variation. Negative stain TEM images of the peptide DFRFRF-NH_2 with 72 mM DA (*A*) and without DA (*B*). Panels *C* and *D* show the peptide RFRFDF-NH_2 with 72 mM DA and without DA, respectively. All samples were prepared at pH 7.8.

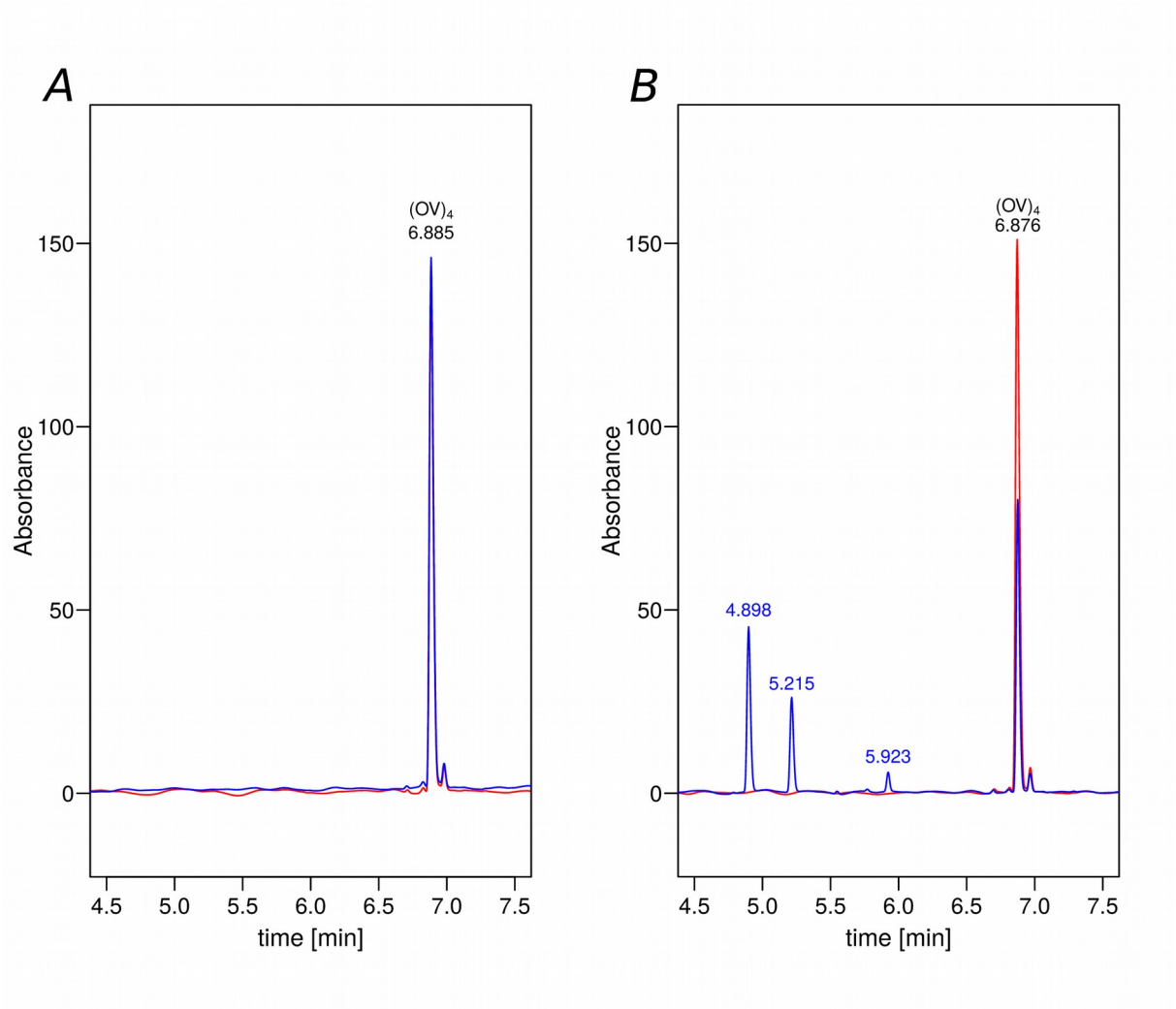

Figure S18. Proteinase K sensitivity of $(OV)_4$ in solution and in the translucent precipititate. HPLC chromatograms of the proteinase K-treated DA-$(OV)_4$ translucent precipitate. (*A*) and $(OV)_4$ alone (*B*). Samples were incubated for 4 hours with (blue trace) or without (red trace) proteinase K. More than half of the peptide is degraded in the absence of DA while no degradation is detected in the presence of DA.

Table S1. Characterization of structural changes for 14 peptides in presence of DA.

Sequence ({Dab} refers to diaminobutyric acid)	0 mM DA		4.5 mM DA		18 mM DA			72 mM DA		
	Appearance[a]	CD[b]	Appearance[a]	CD[b]	Appearance[a]	CD[b]	ATR-FTIR[c]	Appearance[a]	CD[b]	ATR-FTIR[c]
RFRFRFR-NH_2	**C**	max@ 220 nm	**F**	max@ 220 nm	**F**	-	-	**F**	-	**β$^+$**
FRFRFR-NH_2	**C**	max@ 220 nm	**C**	max@ 220 nm	**F**	-	-	**F**	max@ 220 nm	-
DFRFRF-NH_2	**F**	max@ 220 nm	**F**	-	**F**	-	**β$^+$**	**F**	min@ 215 nm	**β^{++}**
RFRFDF-NH_2	**C**	max@ 220 nm	**C**	max@ 220 nm	**F**	-	**β$^+$**	**T**	max@ 220 nm	-
RFRFR-NH_2	**C**	max@ 220 nm	**C**	max@ 220 nm	**T**	-	-	**F**	-	-
RFRFD-NH_2	**C**	max@ 220 nm	**C**	max@ 220 nm	**C**	max@ 220 nm	-	**NC**	max@ 220 nm	-
Ac-VOVAVOVAV-NH_2	**F**	min@ 220 nm	**F**	min@ 220 nm	**F**	min@ 220 nm	**β^{++}**	**F**	**β**	**β^{++}**
Ac-V-{Dab}-VAV-{Dab}-VAV-NH_2	**F**	min@ 190-220 nm	**F**	min@ 197 and 220 nm	**F**	min@ 197 and 220 nm	**β^{++}**	**F**	**β**	**β^{++}**
VOVOVOVOV-NH_2	**C**	**R.C.**	**F**	**R.C.**	**F**	-	**β^{++}**	**F**	**β**	**β^{++}**
V-{Dab}-V-{Dab}-V-{Dab}-V-{Dab}-V-NH_2	**F**	min@ 220 nm	**F**	min@ 220 nm	**F**	-	**β^{++}**	**F**	min@ 220 nm	**β^{++}**
V-{Dab}-V-{Dab}-V-{Dab}-V-NH_2	**C**	**R.C.**	**F**	**R.C.**	**F**	-	**β$^+$**	**F**	min@ 205 nm	**β^{++}**
{Dab}-V-{Dab}-V-{Dab}-V-{Dab}-V-NH_2	**F**	min@ 225 nm	**C**	min@ 225 nm	**F**	-	**β^{++}**	**T**	min@ 220 nm	**β$^+$**
{Dab}-V-{Dab}-V-{Dab}-V-NH_2	**C**	**R.C.**	**C**	**R.C.**	**F**	-	-	**T**	**β**	-
OVOVOVOV-NH_2 „$(OV)_4$"	**C**	**R.C.**	**C**	**R.C.**	**F**	-	**β^{++}**	**T**	**β**	**β$^+$**

Table S1 summarizes the data that is displayed in the subsequent associated panels.

[a] Clear solution is abbreviated as **C**, flocculent precipitate as **F** and translucent precipitate as **T**. In case of no visible change in appearance **NC** symbol is used.

[b] CD spectra are classified as follows: (**R.C.**) has signal indicative of random coil-like structure; (**β**) has signal indicating β-strand structure of peptide; (**-**) signal too weak to interpret; min@ and max@ indicate the wavelengths of maximal and minimal ellipticity in the spectra which do not match any typical secondary structure. In order to better highlight the DA concentration-dependent changes in the CD spectra, in the subsequent associated panels the ellipticities at 197 nm and 219 nm are also separately plotted with grey bars for the signal at 197 nm and black for 219 nm. The dashed lines in the CD spectra mark the position of these two wavelengths.

[c] Strong signal at 1625 cm^{-1} (marked in the spectra with dashed line) is abbreviated as (**β^{++}**), weak signal as (**β$^+$**), no signal as (**-**).

Table S1 Panel 1

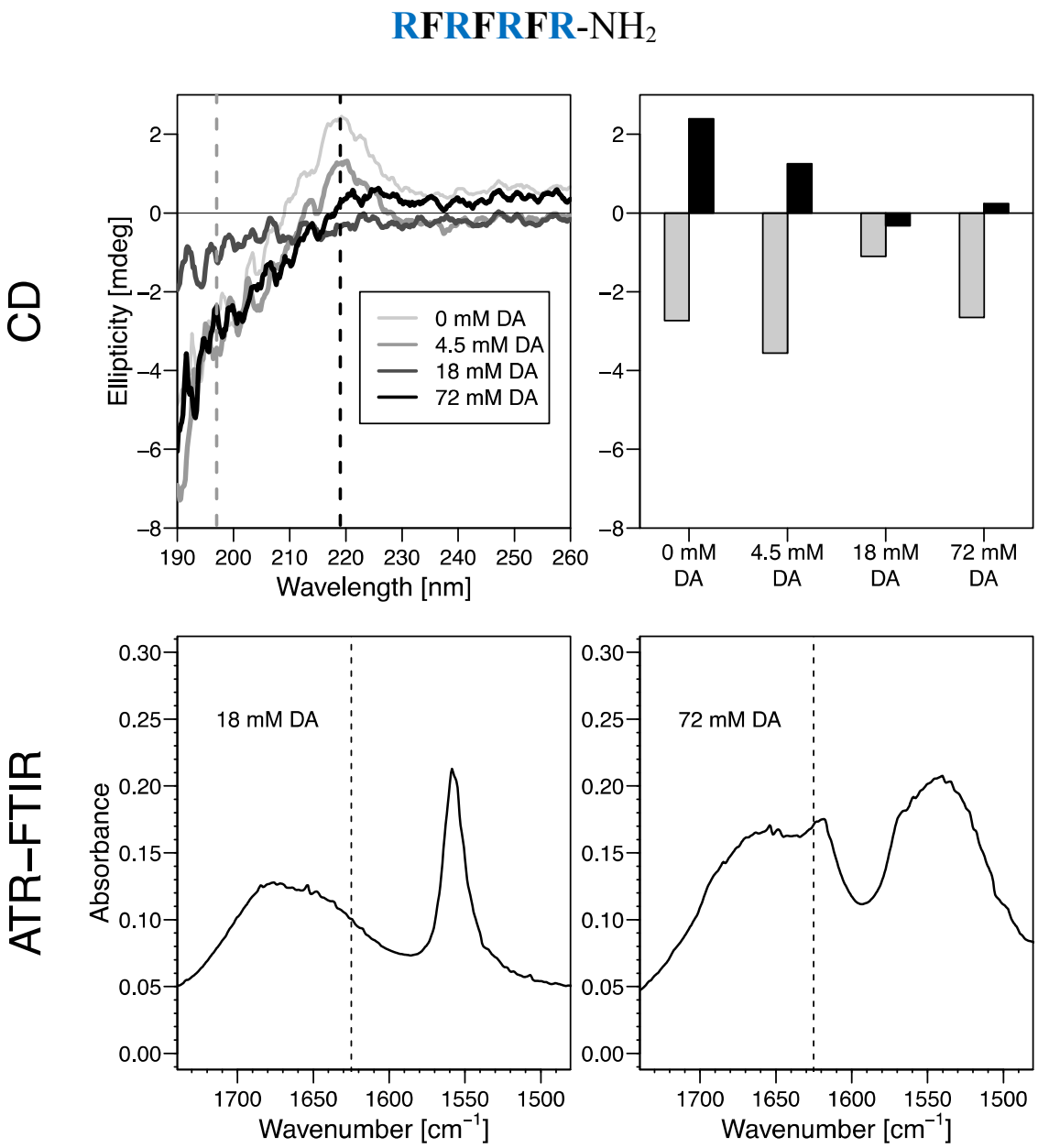

Table S1 Panel 2

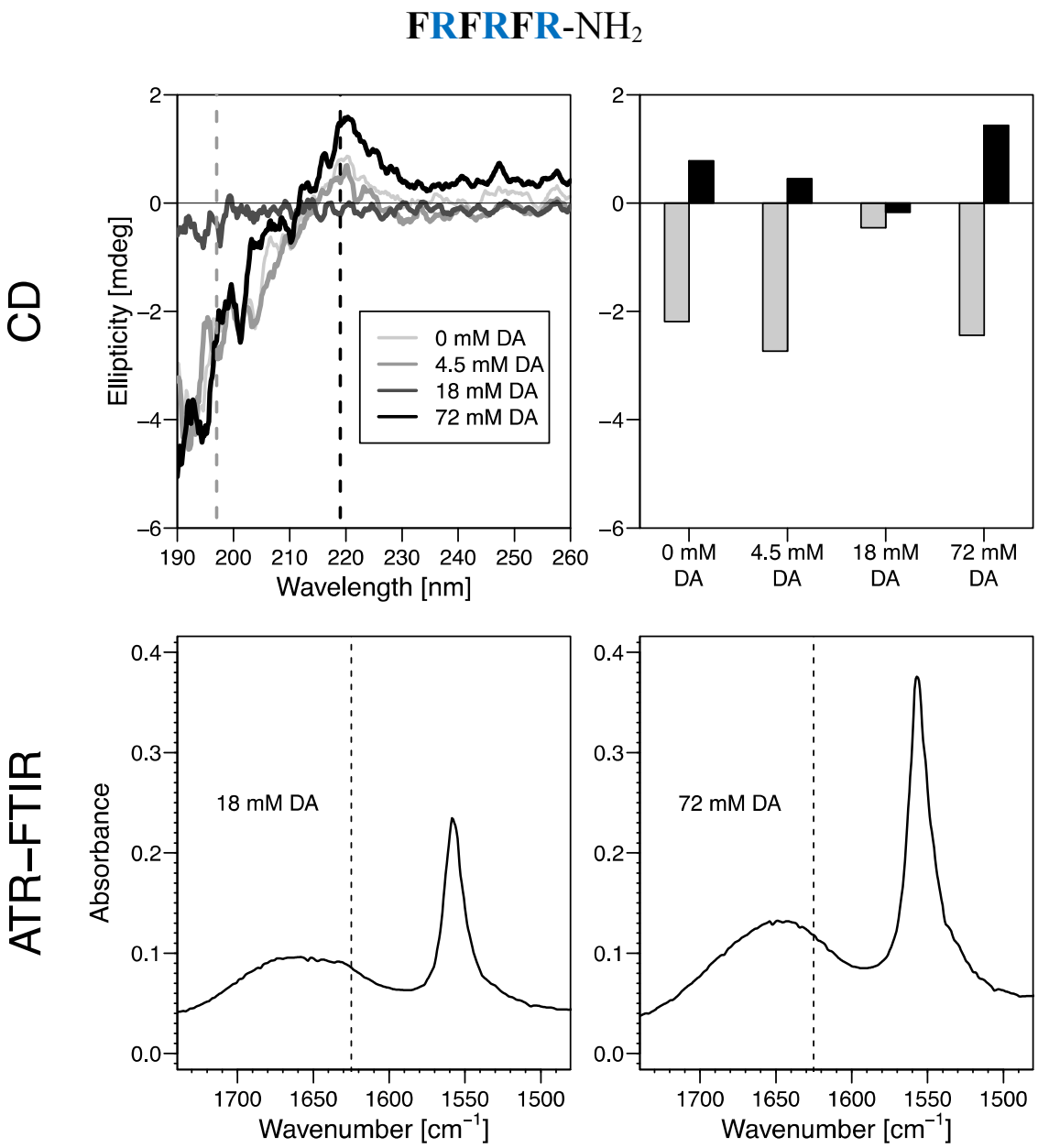

Table S1 Panel 3

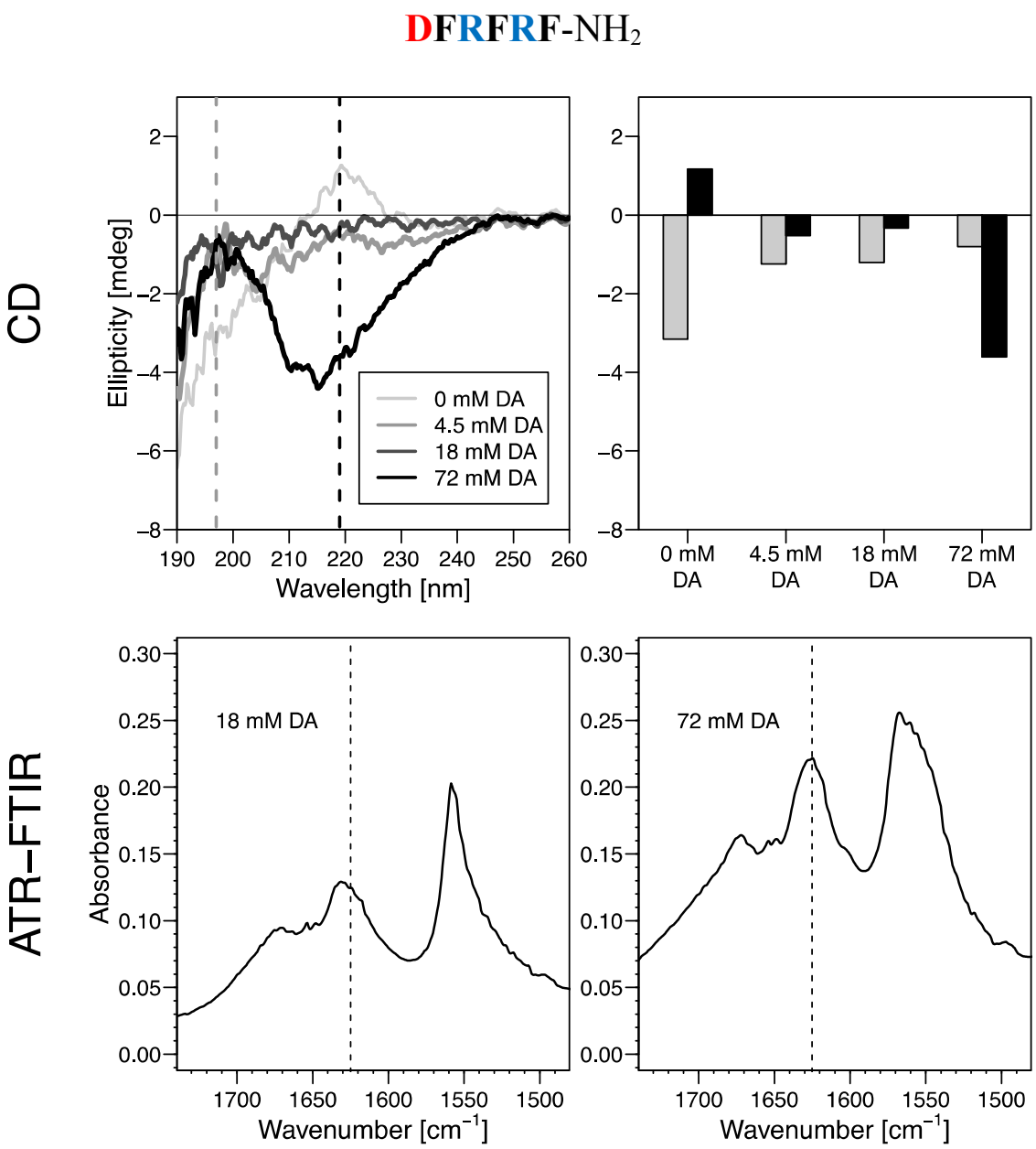

Table S1 Panel 4

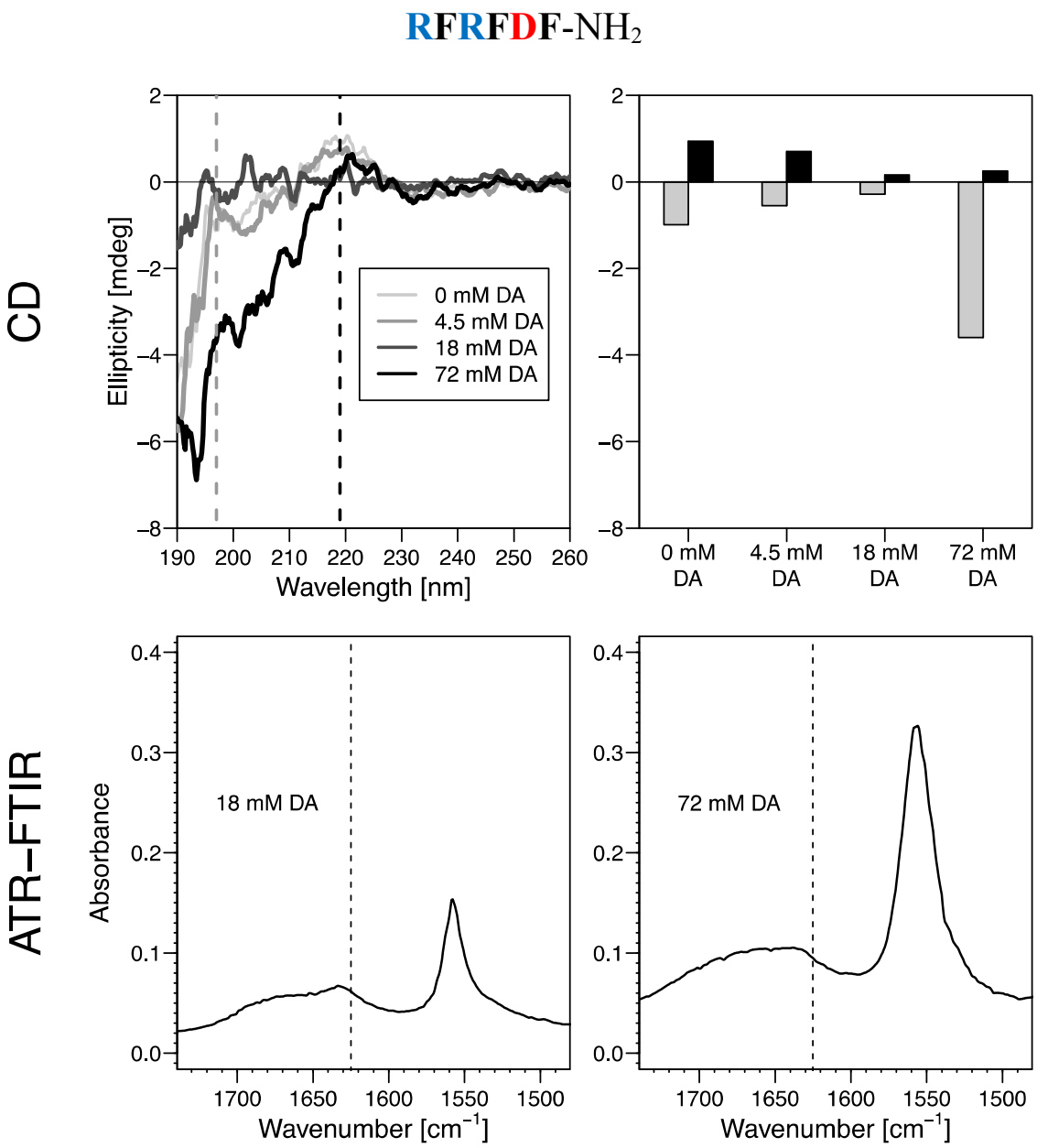

Table S1 Panel 5

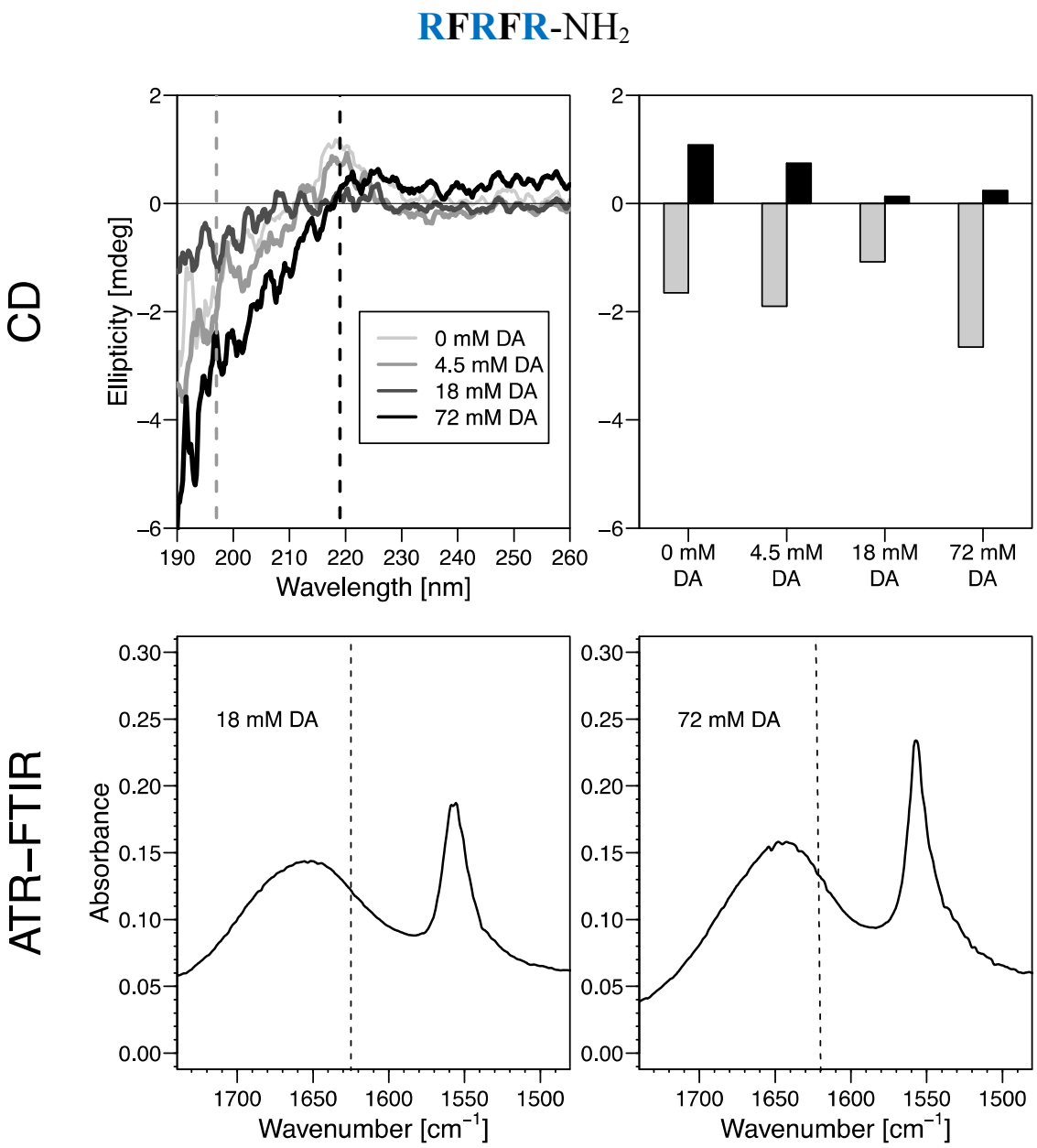

Table S1 Panel 6

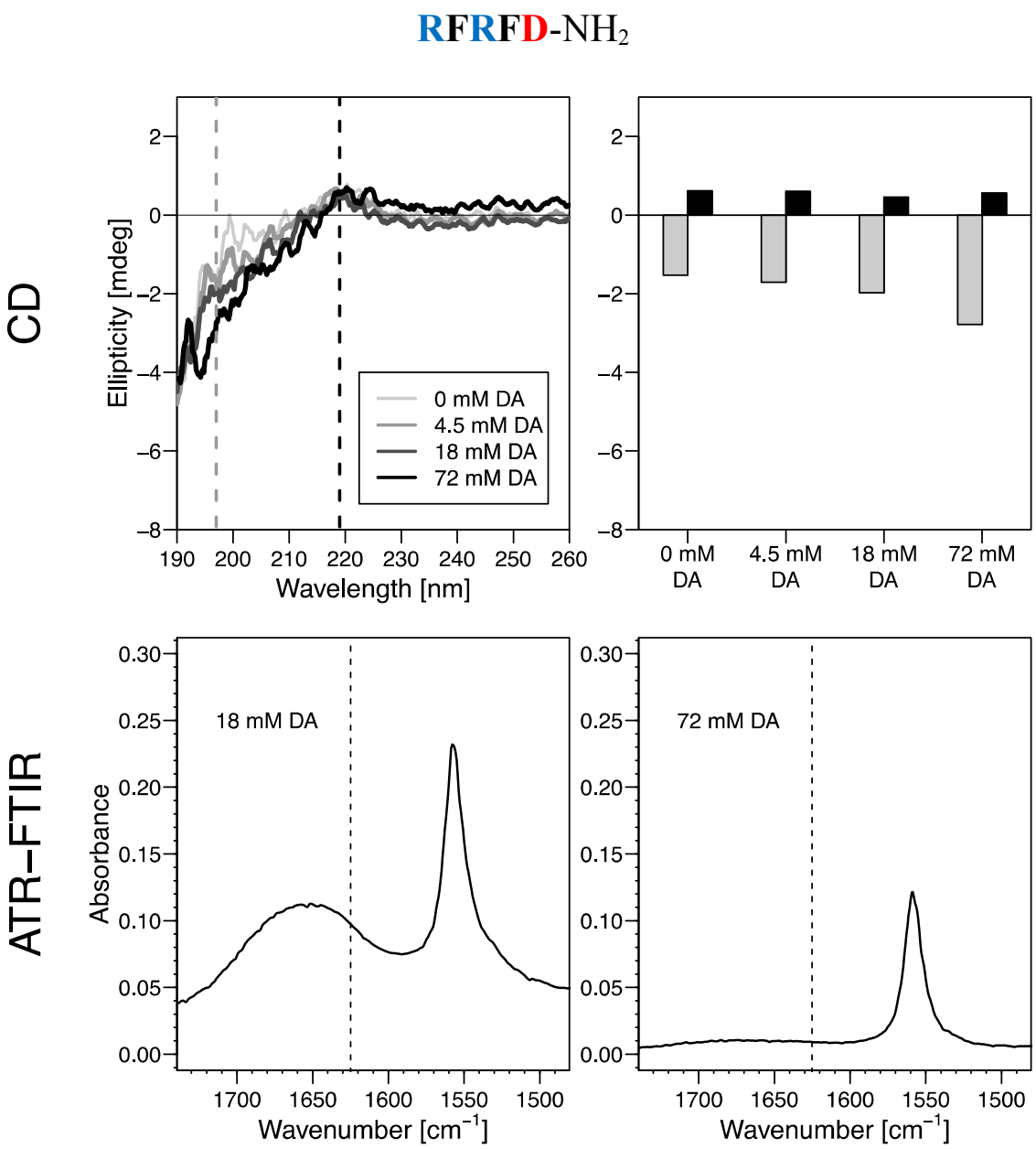

Table S1 Panel 7

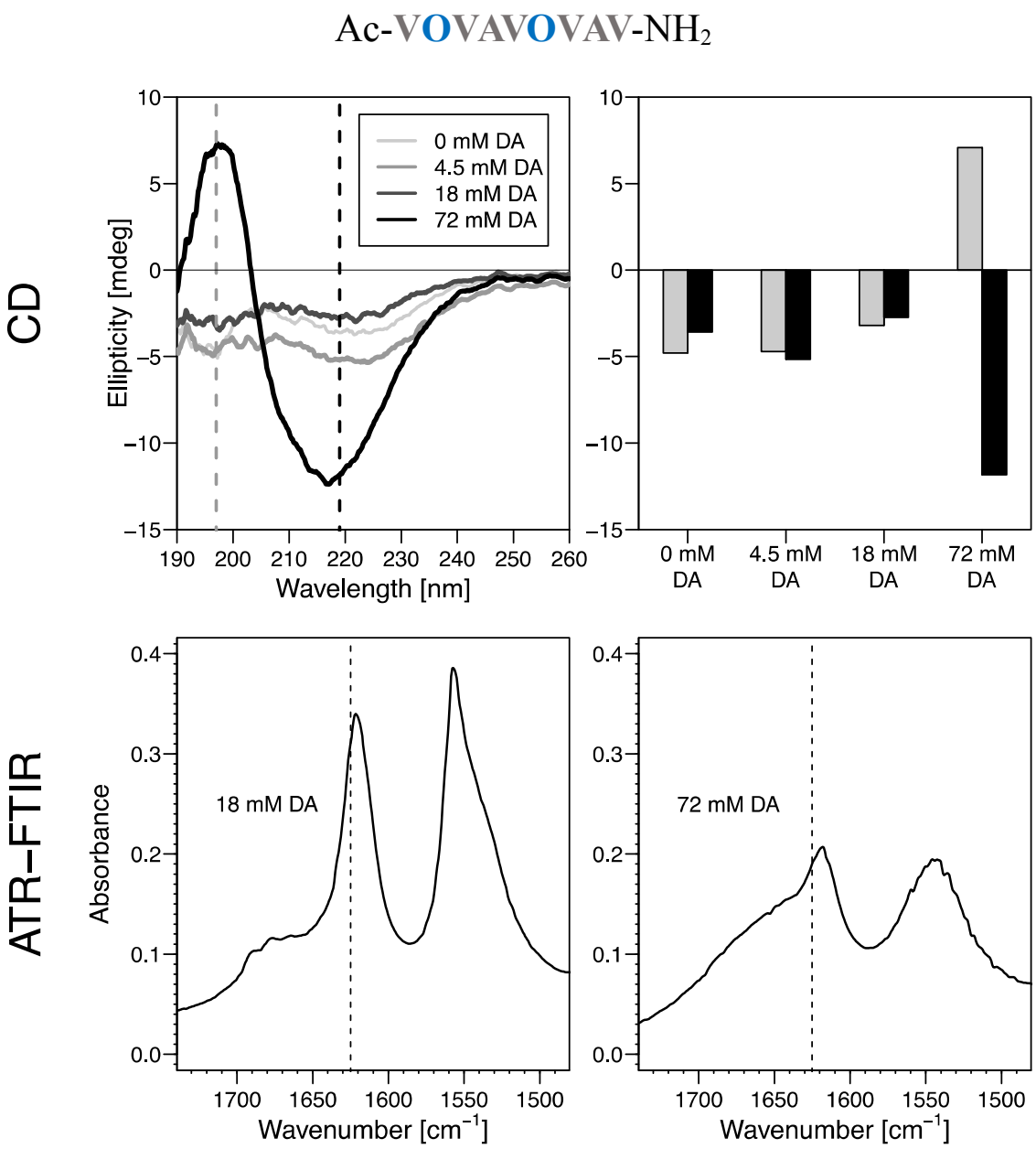

Table S1 Panel 8

Ac-V-{Dab}-V-A-V-{Dab}-V-A-V-NH_2

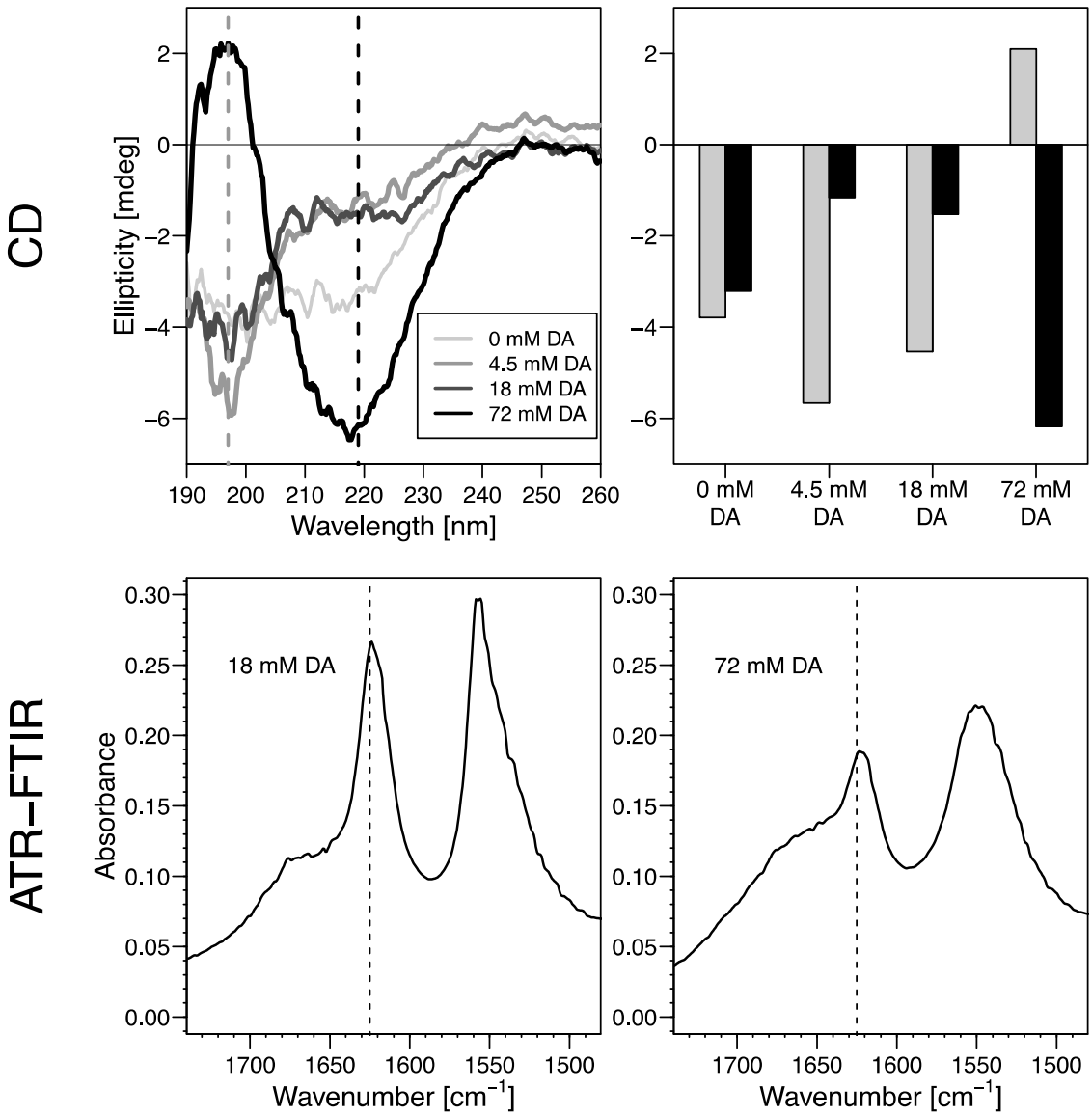

Table S1 Panel 9

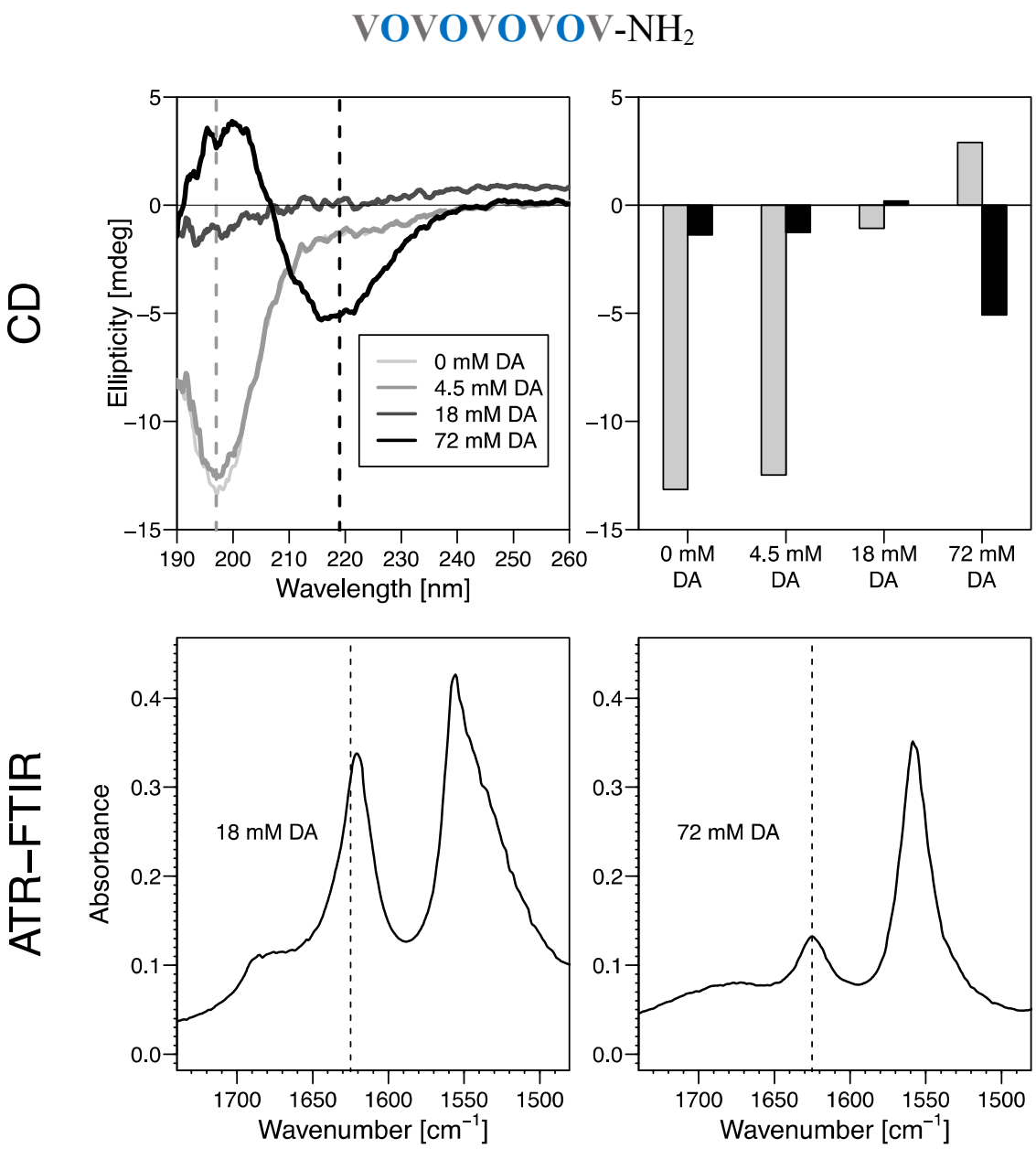

Table S1 Panel 10

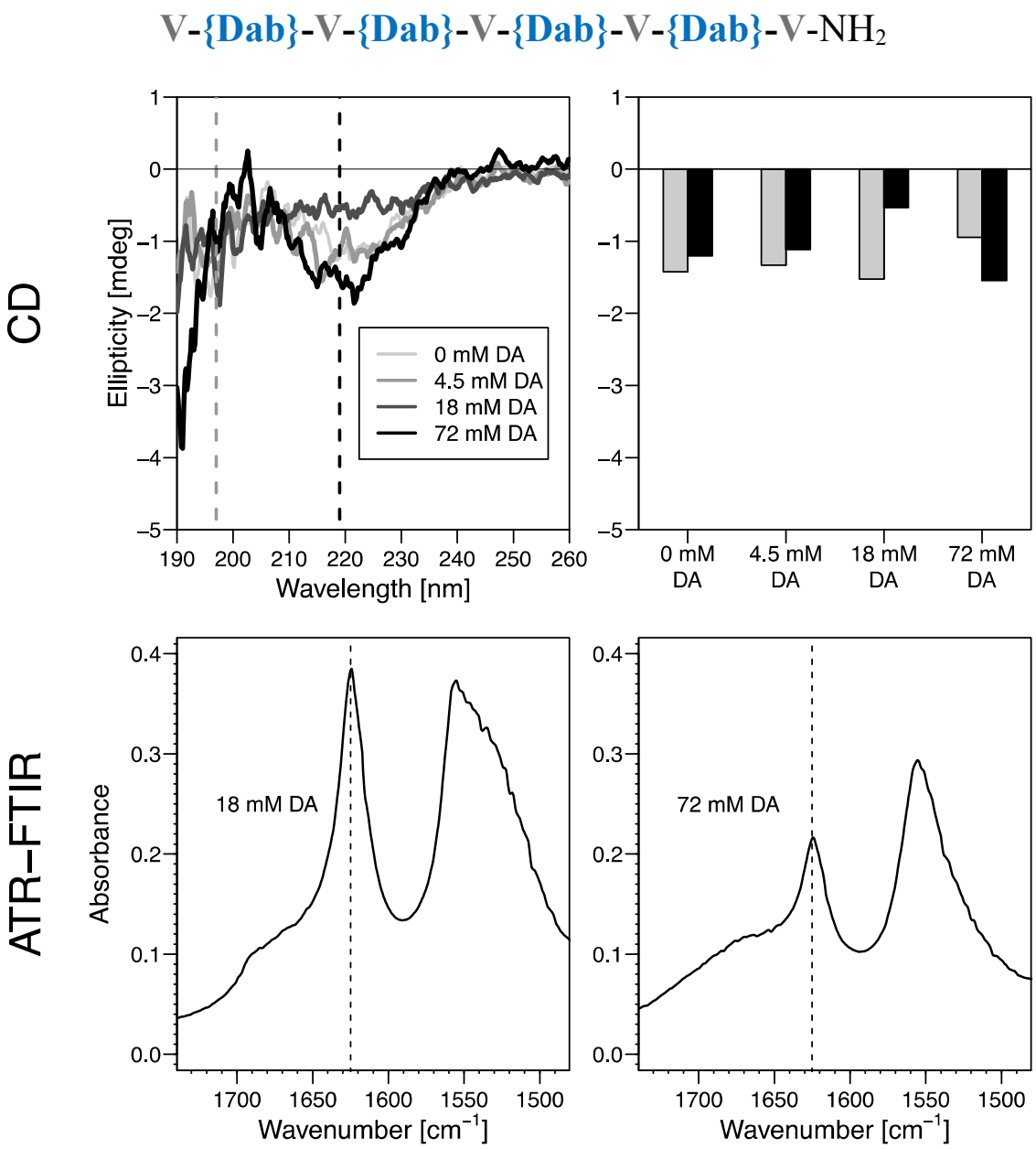

Table S1 Panel 11

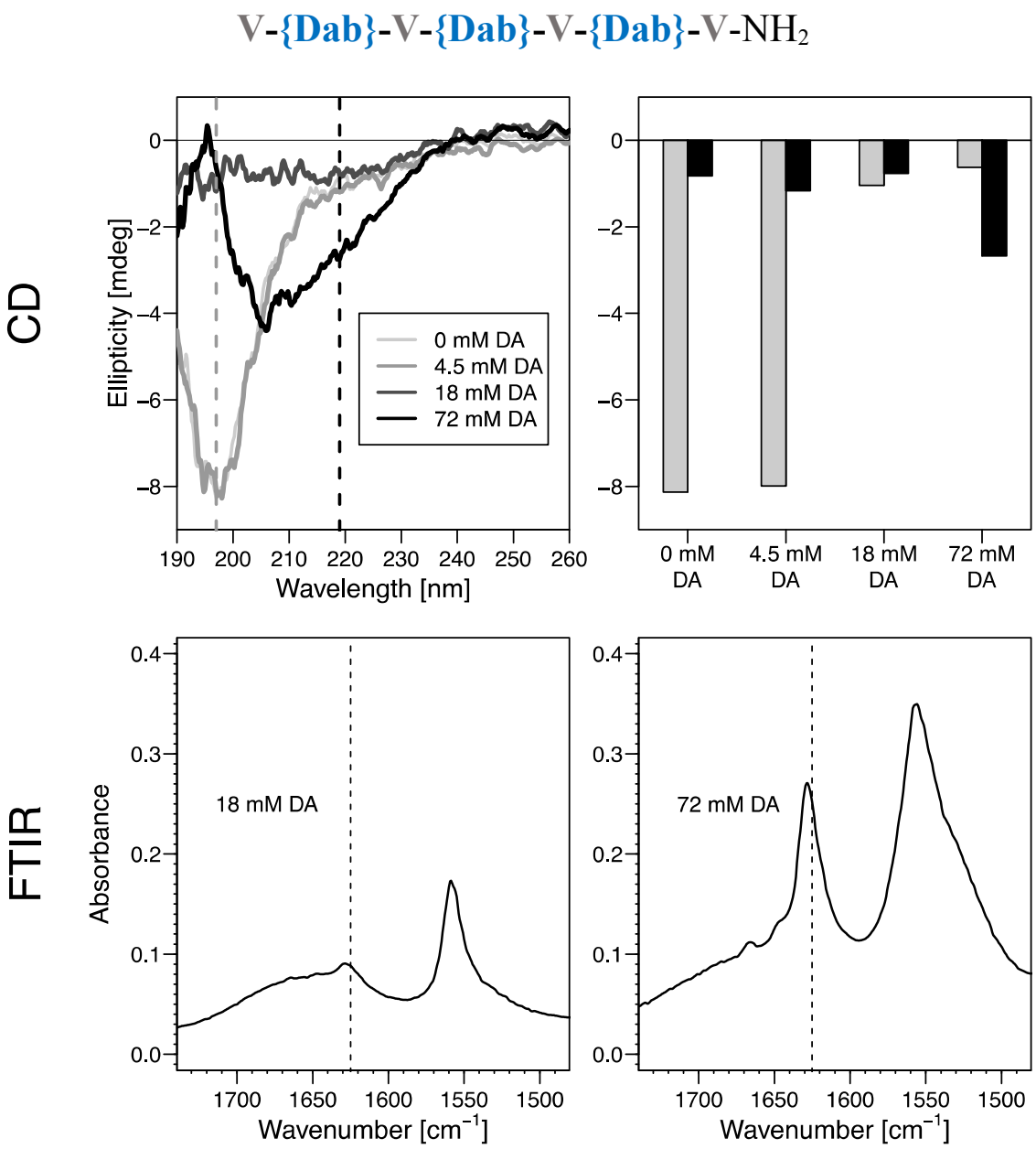

Table S1 Panel 12

{Dab}-V-{Dab}-V-{Dab}-V-{Dab}-V-NH_2

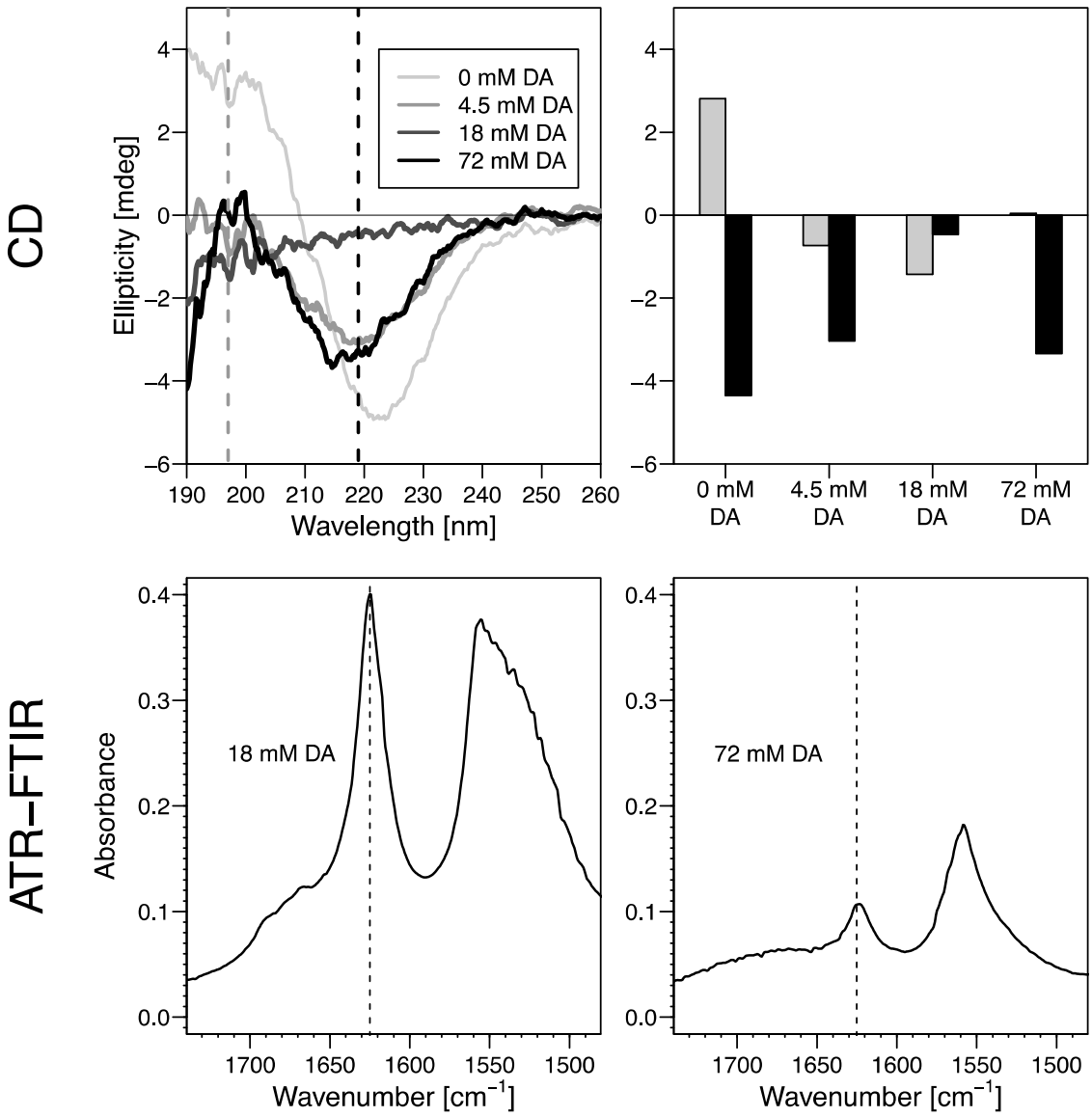

Table S1 Panel 13

{Dab}-V-{Dab}-V-{Dab}-V-NH_2

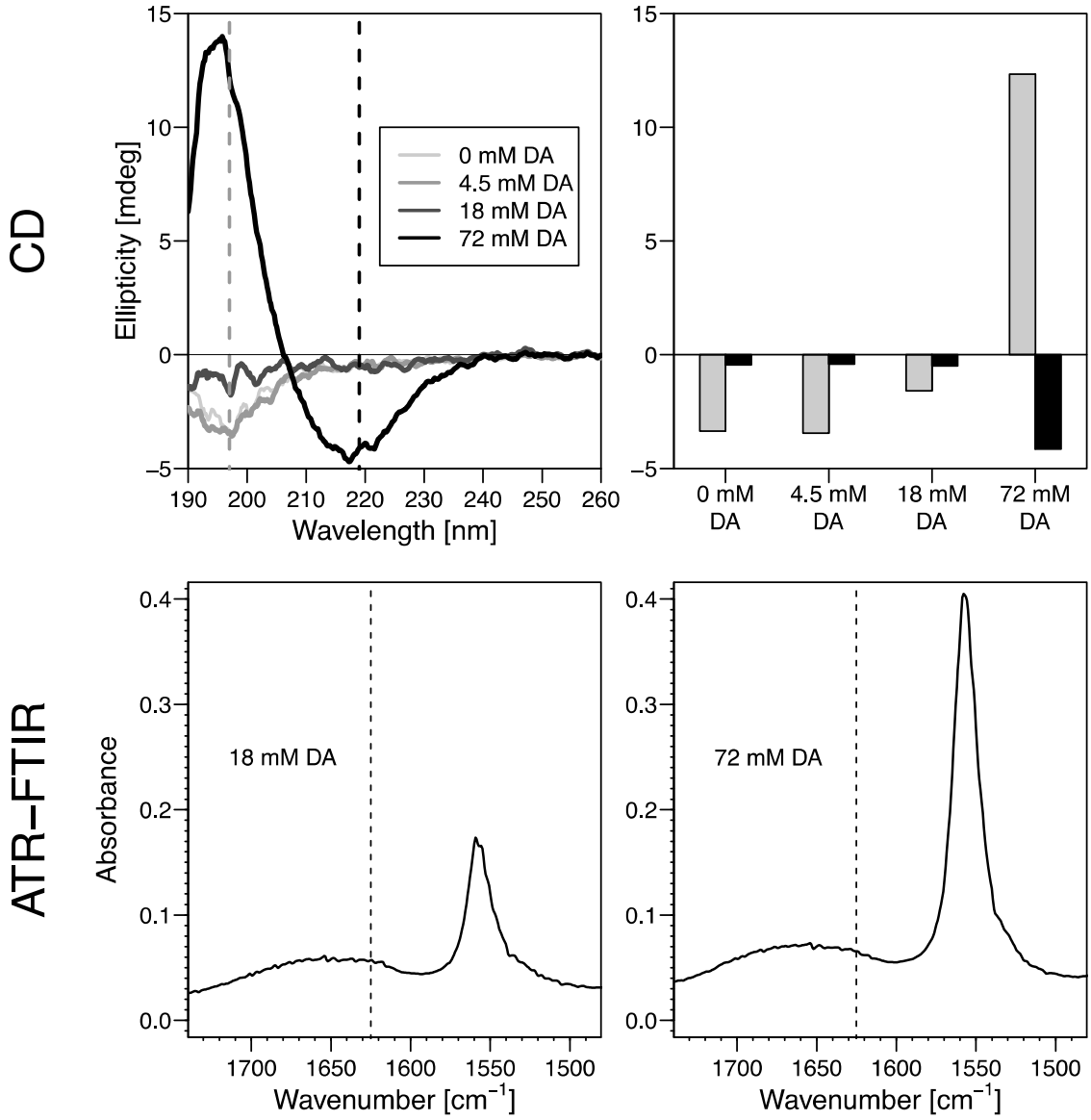

Table S1 Panel 14

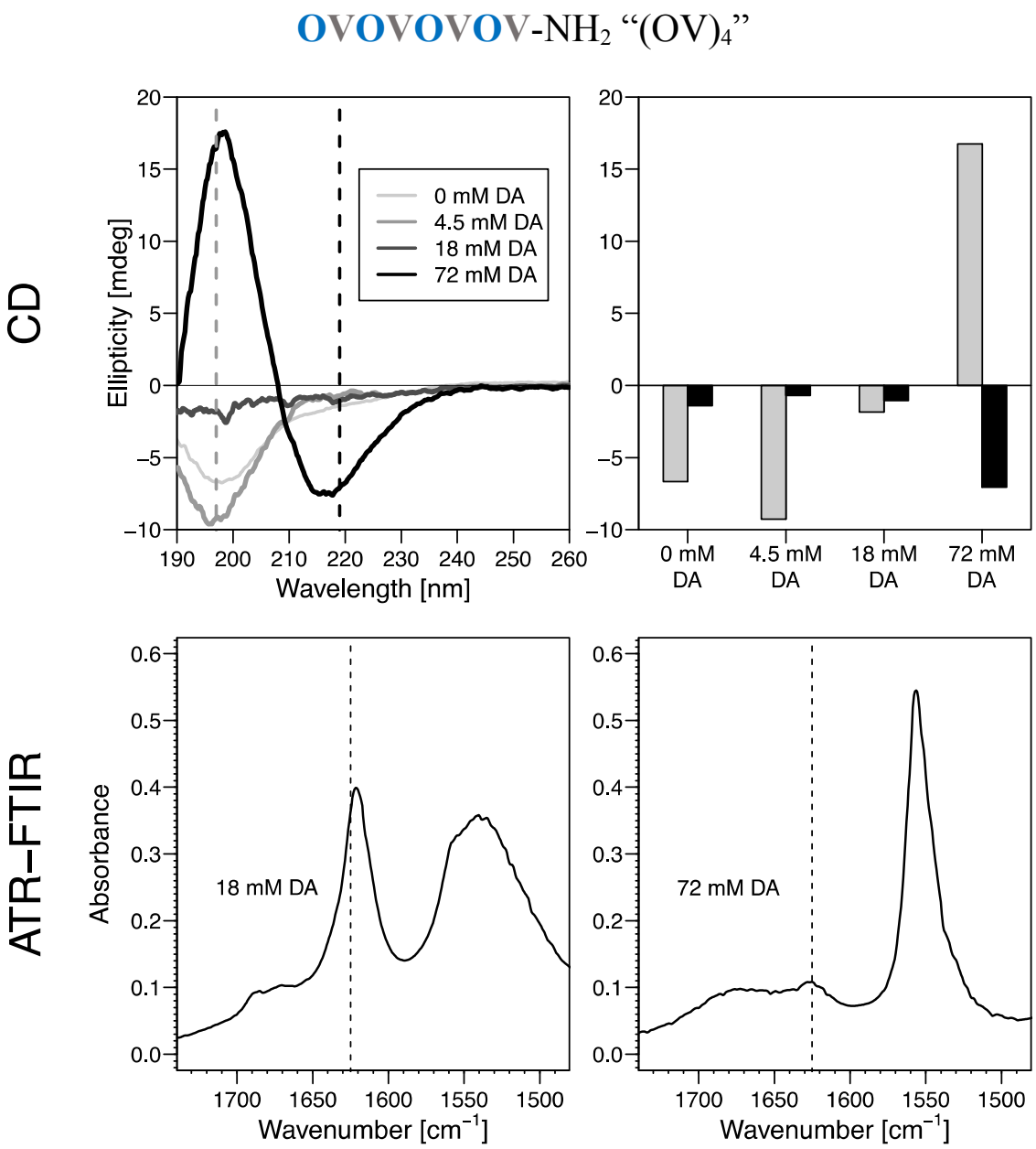

Table S2. Temperature dependence of DPH fluorescence intensity in DA vesicles compared to DA-$(OV)_4$ translucent precipitate.

Temperature	72 mM DA	DA 72 mM/ 575μM $(OV)_4$
25 °C	1 681 700 ± 2100	1 372 300 ± 1700
60 °C	976 100 ± 1800	1 022 500 ± 2400
% decrease[a]	42.0 %	25.5 %

[a] The decrease of fluorescence intensity is attributed to a decreased amount of vesicles at high temperature. The smaller decrease of intensity for translucent precipitate indicates that bilayers of decanoic acid are more stable in the presence of $(OV)_4$.

Form factor for a hollow core two-shell cylinder object

The scattering intensity for a colloidal system can be described as $I(q)=NP(q)S(q)$, where N is proportional to the concentration and scattering volume, $P(q)$ is the form factor, and $S(q)$ is the structure factor.

The form factor for a hollow core two-shell cylinder is described by the following expression:

$$P(q) = k\int_0^{\pi/2}\left[(\rho_{core}-\rho_{in})V_{core}\frac{2J_1(qr_{core}\sin\alpha)}{qr_{core}\sin\alpha}\frac{\sin\left(q\frac{L}{2}cos\alpha\right)}{q\frac{L}{2}cos\alpha}\right.$$
$$+(\rho_{in}-\rho_{out})V_{in}\frac{2J_1(qr_{in}\sin\alpha)}{qr_{in}\sin\alpha}\frac{\sin\left(q\frac{L}{2}cos\alpha\right)}{q\frac{L}{2}cos\alpha}$$
$$\left.+(\rho_{out}-\rho_0)V_{out}\frac{2J_1(qr_{out}\sin\alpha)}{qr_{out}\sin\alpha}\frac{\sin\left(q\frac{L}{2}cos\alpha\right)}{q\frac{L}{2}cos\alpha}\right]^2 sin\alpha\ \mathrm{d}\alpha$$

Where k is the scaling factor, ρ_{core}, ρ_{in}, ρ_{out} and ρ_0 is the scattering length density for the core, inner shell, outer shell and solvent, respectively; V_{core}, V_{in} and V_{out} is the volume of the core, inner shell, and outer shell, respectively; r_{core}, r_{in} and r_{out} is the radius of the core, inner shell and outer shell, respectively; t_{in} and t_{out} is the thickness of the inner shell and outer shell, respectively; and L the length of the cylindrical object.

The relationship between the radii and thicknesses are:

$$r_{in} = r_{core} + t_{in}$$

$$r_{out} = r_{core} + t_{in} + t_{out}$$

The corresponding volumes are:

$$V_{core} = \pi r^2_{core}L$$

$$V_{in} = \pi(r_{core} + t_{in})^2L$$

$$V_{out} = \pi(r_{core} + t_{in} + t_{out})^2L$$